



**National
Oceanography Centre**
NATURAL ENVIRONMENT RESEARCH COUNCIL

National Oceanography Centre

Research & Consultancy Report No. 68

Current and future vulnerability of Argyle International Airport to
combined river & coastal flooding

Benjamin T. Phillips,
Jennifer M. Brown, Amani E. Becker, Andrew J. Plater,

2019

National Oceanography Centre
Joseph Proudman Building
Brownlow St Liverpool
L3 5DA.

Email: benp@noc.ac.uk

© National Oceanography Centre, 2019

Executive Summary

Argyle International Airport is at risk from coastal and fluvial flooding, especially when coarse sediments are deposited in the northernmost tunnel mouths (through which the River Yambou flows) and constrict the carrying capacity. Building on previous research which employed a “bathtub” approach to show areas of St. Vincent at risk from flooding, we use rainfall-runoff, inundation and storm impact models to formulate storm conditions based on Hurricane Ivan, with sea levels representative of the present-day, 2100 (+ 1.10 m) and 2500 (+ 5.48 m) under the Relative Concentration Pathway 8.5 scenario. Combining these with constricted tunnel flow regimes of 20-100% (representing 1-5 tunnels becoming blocked), we assess the risk of flooding to the runway and the rear access road.

We find that the Airport’s drainage system adjacent to the runway copes reasonably well with the applied flood conditions. In present-day and 2100 sea-level scenarios with flow constrictions of $\geq 80\%$, only the northern Runway End Safety Area (RESA) is flooded. However this flooding may be sufficient to render the RESA non-compliant with International Civil Aviation Organisation regulations by reducing its effective width. The greater and more immediate risk is likely to be to the access road which runs around the eastern side of the runway, which is shown to be vulnerable under Hurricane Ivan conditions (a water level of 4.40 m above mean sea level, consisting of astronomical tide, storm surge and wave setup) with no sea-level rise superimposed.

These results must be interpreted with caution as there is no sub-daily precipitation data nor River Yambou flow data, both of which would be required for a more rigorous assessment of the flood risk to the airport. The simplistic representation of the tunnels is also likely to introduce uncertainty by applying an approximate flow solution once the tunnels are full. The main outcome from this work is a modelling framework which could be applied in the future, should better observational data become available to increase the accuracy and robustness of subsequent flood risk assessments.

Contents

1	Introduction	4
2	Data and modelling approach	6
2.1	LISFLOOD-FP: Rainfall runoff and inundation model	7
2.2	XBeach: Storm impact model for sandy coasts	8
2.3	Fluvial discharge through tunnels	8
2.3.1	Digital Elevation Model data	8
2.3.2	Rainfall data	9
2.4	Discharge through tunnels from storm surge and wave set-up. . .	11
2.4.1	Digital Elevation Model data	11
2.4.2	Modelled wave and water level boundary conditions . . .	12
2.5	Modelling flow through the tunnels	13
2.6	Modelling flood propagation on the runway	15
2.7	Modelling flood propagation on the rear access road	17
3	Results	17
3.1	Runway vulnerability	17
3.2	Access road vulnerability	21
4	Conclusions and recommendations	22
5	Acknowledgements	23
A	Runway flood maps	24
B	Access road flood maps	34
C	Models and data availability	64
C.1	XBeach	64
C.2	LISFLOOD-FP	64
C.3	Availability of model data	64

1 Introduction

Previous work by Lichtman et al. (2018) funded by a University of Liverpool Global Challenges Research Fund award identified Argyle International Airport (AIA), St. Vincent & the Grenadines (SVG) as an area vulnerable to coastal and fluvial flooding. However this work only applied a simple “bathtub” approach - where a planar water surface elevation based on several hurricanes plus sea-level rise is intercepted by the terrain’s elevation (Figure 1). Such an approach performs poorly and is shown to inadequately resolve inundation extent when compared with numerical models (Gallien et al., 2018).

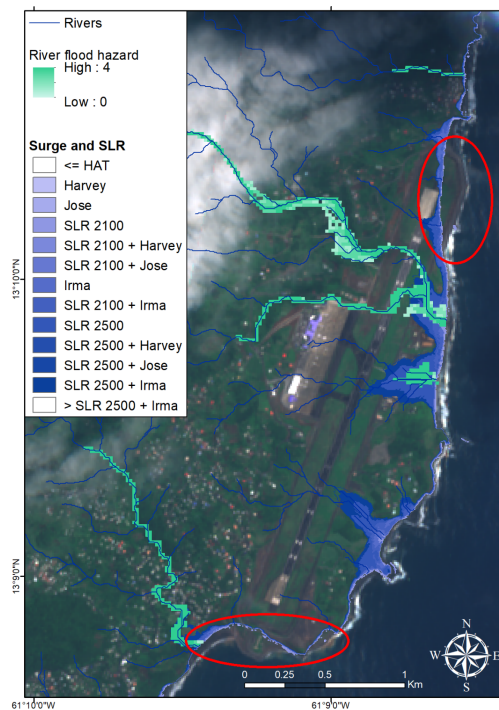


Figure 1: Areas potentially at risk due to sea-level rise and/or storm surge, determined using the “bathtub” method (Lichtman et al., 2018). The red circles show the discrepancy between the Digital Elevation Model (DEM) taken prior to AIA’s construction, and the changes to the area resultant from the land reclamation.

Herein, we use a numerical modelling approach to investigate the threat to AIA from combined flash-flood and storm surge modes of flooding at the northernmost set of tunnels. The River Yambou, which flows through these tunnels has a watershed area of 20 km² and has the potential to deliver boulder-sized sediment leading to sedimentation at the tunnel mouth, causing reduced carrying capacity and an increased risk of flooding to the runway. These risks are

likely to increase in the future, from changes in storm frequency and intensity leading to increases in flash flooding from the River, and the associated sea-level rise reducing the ability of the tunnels to convey river flow.



Figure 2: River Yambou tunnels, looking from the eastern end towards the runway.

Storm surges are caused by low atmospheric pressure systems associated with hurricanes, causing a 1 cm rise in sea level with every 1 hpa decrease in atmospheric pressure. Argyle International Airport, being on SVG's windward coast is also exposed to storm surges and hazardous wind and swell waves, potentially causing additional risk to the airport's sea defences. Wave setup is the super-elevation of the sea surface height above the still water level, driven by gradients in the wave-induced mean moment flux from breaking waves in shallow water (Longuet-Higgins and Stewart, 1964). In this report, we do not investigate the potential for wave overtopping of the airport's rock armour defences, but we do represent the elevated water levels caused by a combination of storm surge and wave setup superimposed on the astronomical tide. To represent sea-level rise for 2100 and 2500, we use the median values from the Relative Concentration Pathway (RCP) 8.5 scenarios from Jevrejeva et al. (2012) of 1.10 m and 5.48 m, respectively. This is consistent with the values applied in the flood maps developed for SVG in response to the Monitoring and Modelling the Coastal Zone: A 3-day interactive training course and stakeholder workshop held in March 2018 (National Oceanography Centre, 2018).

2 Data and modelling approach

Given the paucity of observational rainfall and river flow data, additional modelling work has been carried out to fill in the gaps and provide boundary conditions to explore the vulnerability of the infrastructure to flooding. St Lucia precipitation data was used to formulate two different hydrographs, for which the overall volume of rainfall was the same (representative of Hurricane Ivan) but the duration, peak intensity and time to peak varied. Using LISFLOOD-FP (a flood and rainfall-runoff model), the rainfall profiles were used to model the time-series of discharge through the River Yambou tunnels. The excess discharge once the tunnels reached capacity was combined with storm surge and wave setup conditions (representative of Hurricane Ivan) from regional NEMO and WaveWatchIII modelling was then used to provide conditions to determine the inundation extent under the applied sea-level and tunnel constriction scenarios. Figure 2 provides a visual summary of the applied approach with further detail explained in the following subsections.

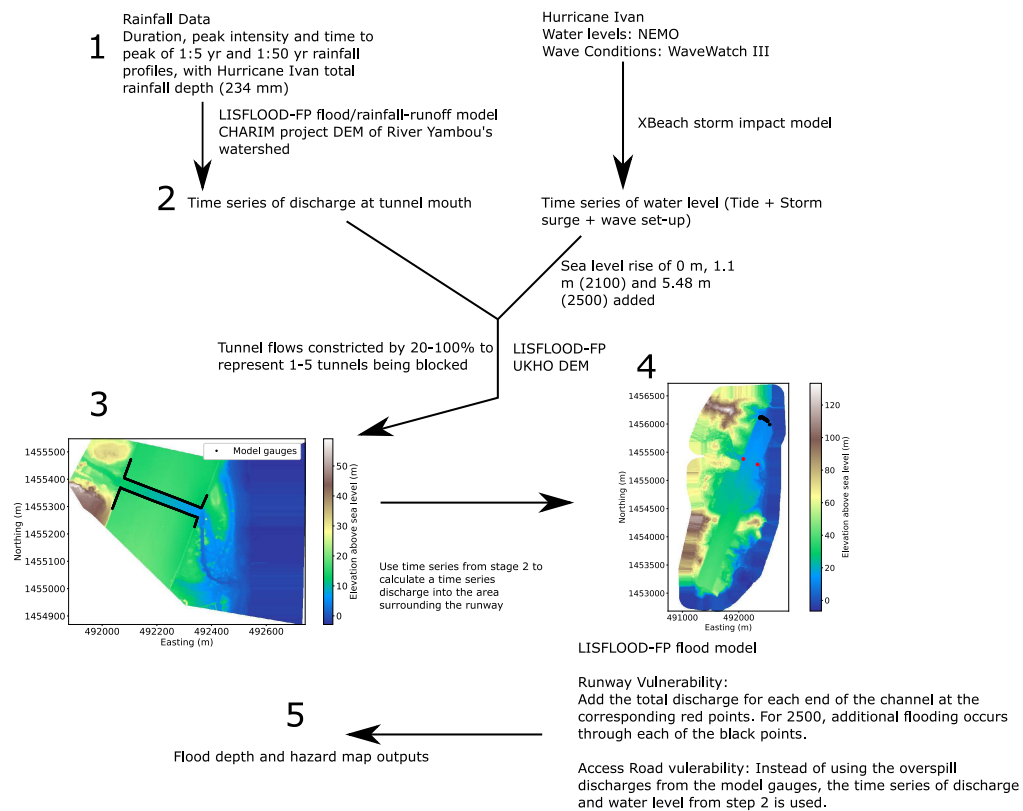


Figure 3: Summary of applied modelling framework

2.1 LISFLOOD-FP: Rainfall runoff and inundation model

LISFLOOD-FP is a two-dimensional, raster-based inundation model, based on a storage cell approach. It is used for fluvial and coastal flooding applications, and has been shown to yield reasonable estimations of inundation extent, at a reduced computational cost (Bates et al., 2005, 2010). It can also be used to resolve rainfall runoff, and has a specific solution to ensure numerical stability on steep-sided slopes (Sampson et al., 2013), making it an appropriate model for application to the River Yambou’s watershed.

It is important to note the following limitations of the model.

1. It is an open channel model usually used for coastal and fluvial applications. The model physics only apply to compressible flows, hence once the tunnels are full, a solution for open channel flow rather than pressurized pipe flow applies.
2. It does not resolve geomorphic processes. It therefore cannot determine the volume of sediment delivered to the tunnel mouths by rainfall runoff or how the DEM might be altered throughout the storm from erosion or deposition, and subsequent changes in channel conveyance. This is a limitation of most commonly applied flood models, and is not unique to this study.
3. Whilst capable of using either water elevation or water discharge as input, it does not resolve waves and therefore will not capture any inundation resulting from processes such as splash of river flow overtopping the bridge. It will only capture overflow of the still water level when it exceeds the elevation of the tunnel-equivalent channel or the coastal defences.
4. We consider all grid cells with a water depth of < 0.05 m to be dry to account for the vertical accuracy of the applied DEM. This is commonly applied to studies of a similar type (e.g. Prime et al., 2016).

LISFLOOD-FP contains a parameter to calculate the maximum Flood Hazard Rating (FHR, a function of water depth and velocity) experienced in each grid cell throughout the simulation. It is calculated according to the UK’s Department for Environment, Food and Rural Affairs methodology (Surendran et al., 2008), as follows:

$$V_c = \sqrt{V_x^2 + V_y^2} \tag{1}$$

$$FHR = \max[D \times (V_c + 1.5)] \tag{2}$$

where V_x and V_y are velocities in east/west and north/south directions, respectively. V_c is the resultant cell velocity, D is water depth in the grid cell and 1.5 is a constant debris factor. FHR is then classified according to the following table:

Table 1: Flood hazard rating methodology (Surendran et al., 2008).

FHR Value	Degree of flood hazard	Description
< 0.75	Low	Caution – shallow flowing or deep standing water
0.75 - 1.25	Moderate	Dangerous for some e.g. children, elderly etc.
1.25 - 2	Significant	Dangerous for most people
> 2	Extreme	Dangerous for all (including emergency services)

2.2 XBeach: Storm impact model for sandy coasts

XBeach is an open-source physics-based model designed to resolve hydrodynamic and morphodynamic processes on sandy coasts, over event time scales and areas in the order of kilometers. XBeach solves coupled 2D horizontal equations for wave propagation, flow and sediment transport for wave and tidal boundary conditions (Roelvink et al., 2009). It has been shown to effectively hindcast storm impact, overwash and breaching on sandy dunes. It has also been used in the operation of coastal impact forecasting systems. Whilst capable of resolving both cross-shore and longshore processes, in this study we use it in 1D mode (cross-shore) only, with morphological evolution disabled. Other models such as SWAN would provide longshore variable wave setup values, however given the narrow section at the mouth of the River Yambou that this study concerns, XBeach is an appropriate model to apply in this study.

2.3 Fluvial discharge through tunnels

There is a lack of observational flow data for the River Yambou, and often gauges are destroyed during intense storms, providing an inaccurate measure of river discharge even where observational infrastructure exists. In order to understand the response of the Yambou watershed to extreme rainfall, we apply LISFLOOD-FP to resolve rainfall runoff in the watershed and the resultant river flow at the mouth of the tunnels. There is therefore a large amount of uncertainty in the watershed’s response to extreme rainfall events.

2.3.1 Digital Elevation Model data

For modelling rainfall runoff, we use the LiDAR Digital Elevation Model (DEM) which was applied in the original “bathtub” flood risk assessment (Figure 4). The vertical accuracy, whilst not stated on the website, is likely to be around ± 0.15 m and the spatial resolution is 5 m. To effectively model rainfall run-off, a DEM of the entire watershed is required, meaning the high resolution UKHO survey carried out by the UK Hydrographic Office was inappropriate due to its lack of coverage. The Caribbean Handbook on Risk Information Management (CHARIM) DEM was taken prior to the construction of AIA airport, however is suitable for determining flow in the proximity of the tunnels from rainfall runoff (location marked on Figure 4).

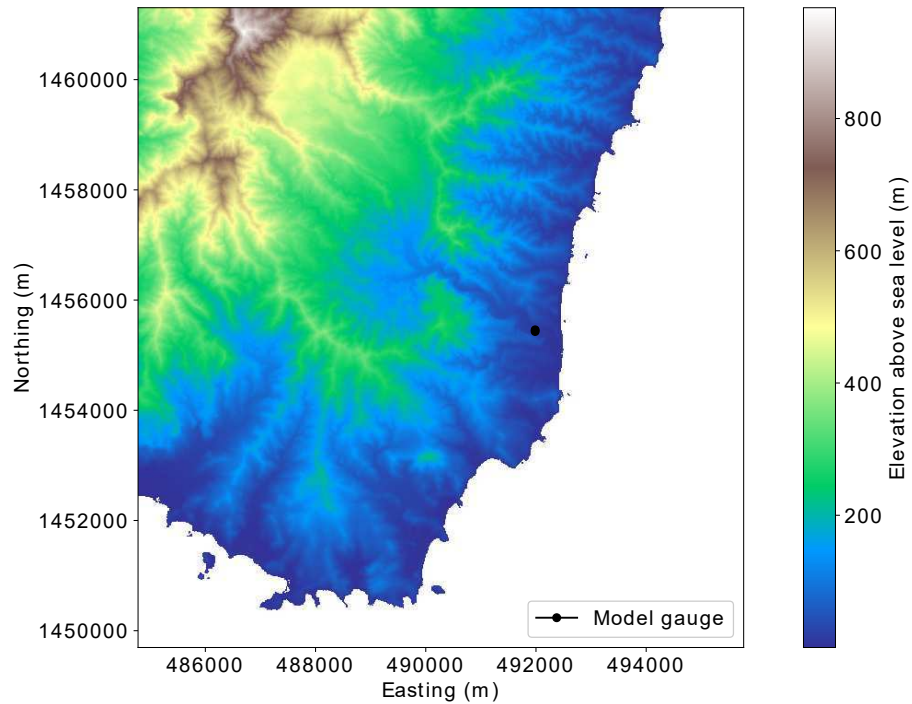


Figure 4: Applied DEM used for the rainfall runoff modelling.

2.3.2 Rainfall data

We selected Hurricane Ivan as the event to model rainfall runoff and the resulting discharge into the tunnels, as it was the largest recorded rainfall event for SVG. SVG Met Office only holds daily precipitation data, which is too infrequent to derive synthetic rainfall events which last in the order of hours. Previous work was carried out in the Caribbean Handbook on Risk Information Management (CHARIM) project to derive design storm events for SVG using one minute rainfall intensity data from St Lucia.

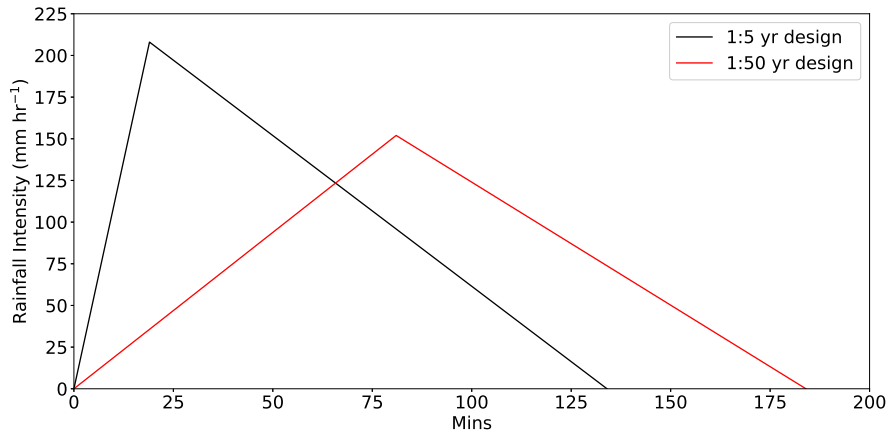


Figure 5: Applied rainfall events for determining discharge into the tunnels. Duration, peak intensity and time to peak are from 1:5 yr and 1:50 yr rainfall profiles from St Lucia, however the overall rainfall depth is 234 mm in both scenarios.

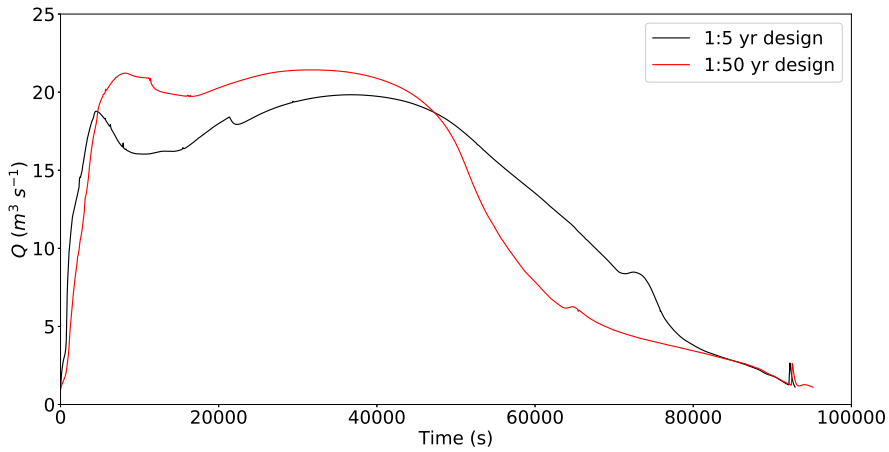


Figure 6: Modelled time series of river discharge through the model gauge shown on Figure 4 using LISFLOOD-FP, for the two rainfall profiles shown above.

LISFLOOD-FP applies a spatially uniform rainfall field to the DEM, and linearly interpolates a value at each model time step. The user can also set a virtual gauge for a given grid cell (or series of grid cells) for which discharge

through the cell can be saved at a user-specified interval. Here we save a time series of discharge at the location marked on Figure 4. This location is slightly upstream of the tunnel mouths due to the discrepancy in the river channel geometry between the CHARIM and UK Hydrographic Office (UKHO) surveys, recorded before and after modifications to the river channel were made during the runway’s construction. We are unable to carry out any rigorous model validation due to a lack of monitoring data regarding flow of the River Yambou, as such there is a large amount of uncertainty. Instead we carry out sensitivity analysis using rainfall characteristics (peak intensity, time to peak and duration) of two different design storms, but maintaining an equal overall rainfall total of 234 mm, the highest recorded daily rainfall (Hurricane Ivan, September 2004) at the E.T. Joshua Airport station.

We therefore derived the two hydrographs shown on Figure 6 as follows:

- Hydrograph 1: The discharge at the tunnel mouths resulting from the characteristics of a 1:5 yr design rainfall event. Overall rainfall total = 234 mm.
- Hydrograph 2: The discharge at the tunnel mouths resulting from the characteristics of a 1:50 yr design rainfall event. Overall rainfall total = 234 mm

The purpose of applying multiple design hydrographs is to explore how the variability in duration and peak intensity of the rainfall might affect the discharge through the tunnels, and the resultant inundation extent and flood hazard rating.

2.4 Discharge through tunnels from storm surge and wave set-up.

2.4.1 Digital Elevation Model data

Here we use the bathymetric LiDAR (1 m spatial resolution) collected by UK Hydrographic Office as part of the Commonwealth Marine Economies Programme (CMEP). As opposed to the DEM collected by the CHARIM survey, this covers the airport and the runway. Limitations of this survey are as follows:

1. Since the survey was focussed on capturing bathymetry, it is inclusive of surface features such as buildings and vegetation. This reduces the accuracy for example where beaches are vegetated or trees overhang river channels. Features such as this, and bridges which would obstruct flow, were manually digitized out of the DEM.
2. Due to the steep shoreface on the windward coast of SVG, the LiDAR is unable to survey some areas as they are too deep. Missing values were interpolated into the DEM, which introduces some uncertainty into the beach profile used to determine wave setup.

2.4.2 Modelled wave and water level boundary conditions

As part of the Ocean modelling and monitoring for Caribbean Small Island Developing States project, funded by the CMEP, Caribbean-wide wave (WaveWatchIII) and water level (NEMO) models were applied to hindcast wave and surge conditions for several hurricanes, including Hurricane Ivan. Using modelled boundary conditions for Hurricane Ivan (Figure 7), XBeach was applied in the cross-shore direction using a beach profile extracted from the UKHO survey, to produce a time-series of water elevation resultant from storm surge and wave setup (Figure 8), which is then used as input to model flow through the seawards end of the tunnels. The temporal resolution of this time series is one minute, which comprise a water level (astronomical tide + storm surge) interpolated from hourly NEMO output, combined with the maximum wave setup for each minute.

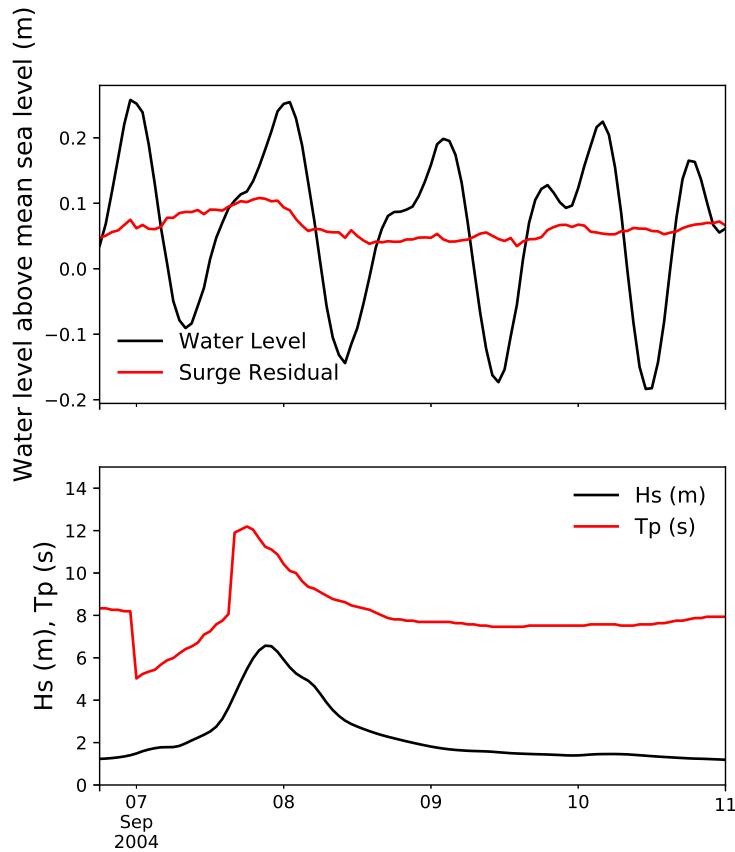


Figure 7: Modelled wave and water level (astronomical tide + storm surge) conditions during Hurricane Ivan, from WaveWatchIII and NEMO.

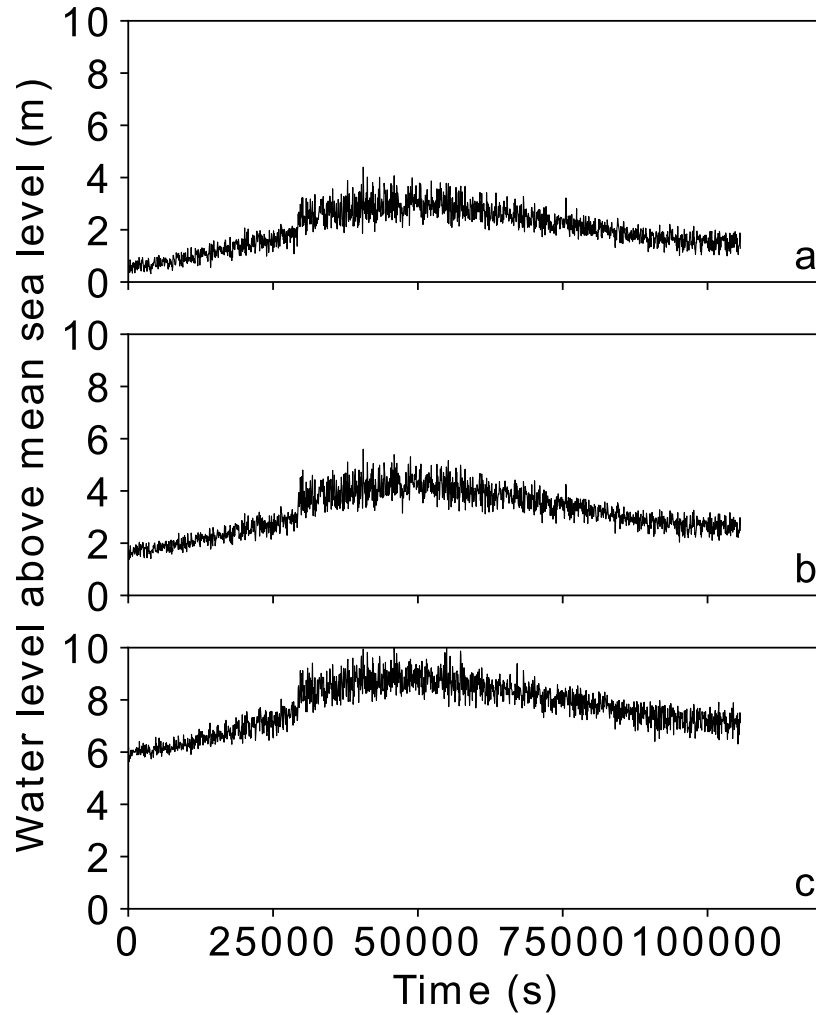


Figure 8: Modelled water level (sum of astronomical tide, storm surge and wave setup components) for the conditions in Figure 7 under a) present-day sea level, b) 2100 sea level (+ 1.10 m) and c) 2500 sea level (+ 5.48 m).

2.5 Modelling flow through the tunnels

Combining the modelled River Yambou discharges under the design hydrographs (Figure 6) with the modelled water levels (Figure 8) yields multi-modal flood conditions for Hurricane Ivan. We then superimpose sea-level rise values of 0 m, 1.1 m and 5.48 m on to the modelled water levels to represent the present-day, 2100 and 2500, respectively. This then gives six different sets of flooding conditions shown in Figure 9.

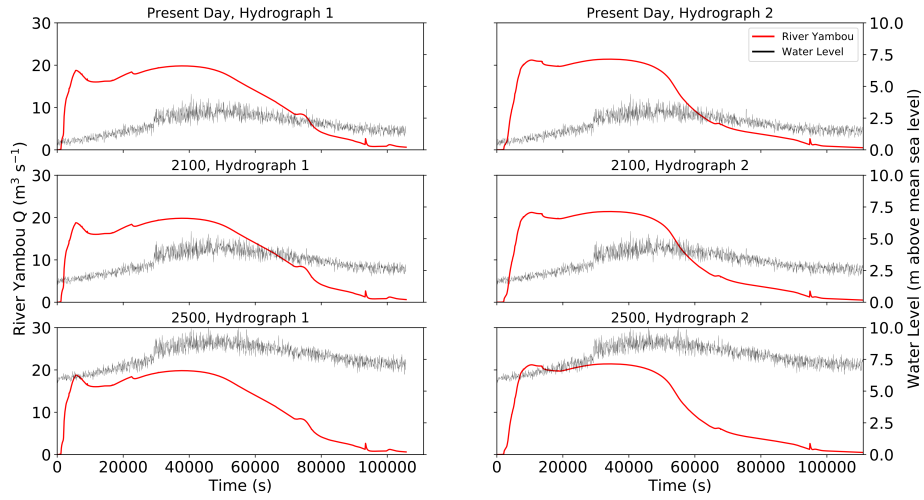


Figure 9: Applied boundary conditions for the LISFLOOD-FP flood model: Hydrographs 1 and 2 (as described in Section 2.3.2) represent the River Yambou, and modelled water levels as shown in Figure 8 under the present-day, 2100 and 2500 sea-level scenarios.

We calculate the volume (V) of each tunnel following:

$$V = D^2 \eta L = 9965 \text{ m}^3 \quad (3)$$

where $D = 6.1$ m (diameter of tunnel), $\eta = 0.8927$, an areal factor for D-shaped tunnels and $L = 300$ m (length of tunnel). Multiplying V by 5 gives an overall carrying capacity of 49826 m^3 combined capacity for all tunnels. We then treat the tunnels as an equivalent open channel, by manually digitizing into the DEM a channel with this capacity (Figure 10).

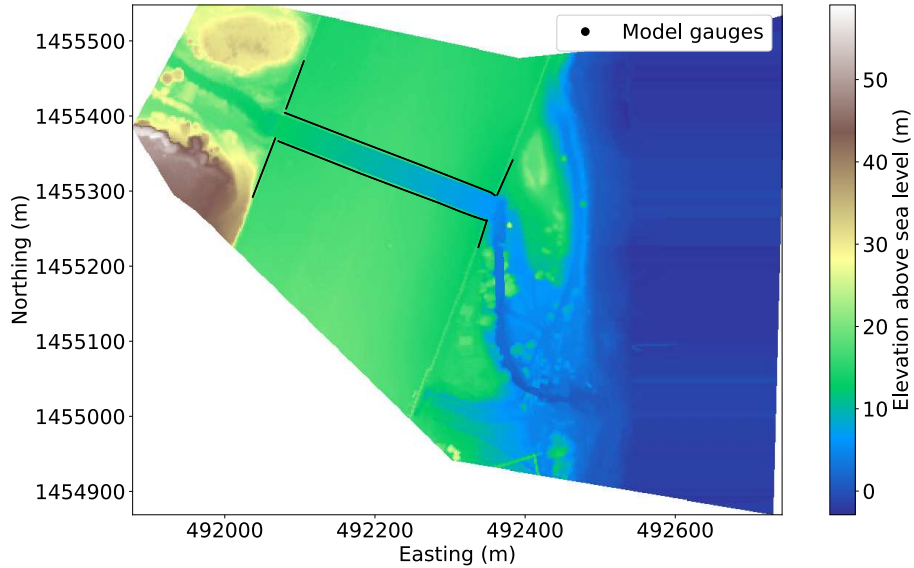


Figure 10: Applied DEM for modelling river flow through the tunnels. Derived from UK Hydrographic Office survey with a spatial resolution of 1 m. Missing values have been interpolated.

Treating the tunnels as a rectangular cuboid, since LISFLOOD-FP uses a rectilinear grid and is unable to resolve the geometry of the D-shaped tunnels, we calculate the height (H) as:

$$H = \frac{V}{D L} = \frac{49826}{30 \times 300} = 5.53 \text{ m} \quad (4)$$

We then systematically reduce the size of this channel in 20% increments by increasing the river bed elevation, to mimic the failure of tunnels from sediment deposition. We then use virtual gauges in LISFLOOD-FP along the banks of the channel, and parallel to the runway to determine the time-varying discharge of overspill onto the runway, for each of the aforementioned channel capacities, for each of the river & water level scenarios shown in Figure 9.

2.6 Modelling flood propagation on the runway

LISFLOOD-FP is then used to model the resultant inundation onto the runway, using a DEM without the channel included (Figure 11). Under present-day and 2100, at the northern end of the runway, defences are not shown to overspill, and therefore the only access route for flood water is from the failure of the tunnels. Under the 2500 sea-level scenario, the water level elevation exceeds the crest

height of the defences, creating an additional mechanism for flooding, which needs to be accounted for in the modelling. We account for this as follows:

- Present-day and 2100: For each scenario, discharges in the direction of runway were calculated for each model gauge on Figure 10, and are assumed to represent excess water once the maximum conveyance of the tunnels is reached. This discharge enters the runway at the red points on Figure 11, representative of the ends of the channel.
- 2500: As described above, however flood water from the black gauge points along the northern end of the runway are also added.

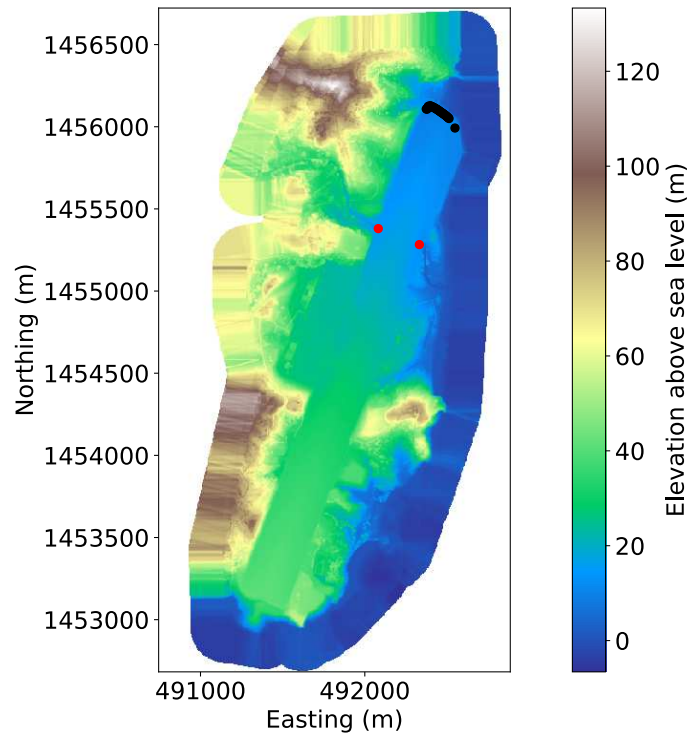


Figure 11: Applied DEM for modelling the propagation of overspilled flood water onto the runway. Derived from UK Hydrographic Office survey with a spatial resolution of 5 m. Missing values have been interpolated. Red dots show the points at which the River Yambou discharge and discharge from storm surge and wave setup is added from the western and eastern ends of the tunnel, respectively. Black dots show the additional gauge points required to capture the additional water entering the area from elevated sea levels overflowing the defences, and are applied in the 2500 sea-level scenario only.

2.7 Modelling flood propagation on the rear access road

Flooding of the rear access road could occur regardless of the condition of the tunnels from elevated water levels during storm surges. Determining the flood extent therefore demands an alternate approach from the one used to model flood inundation on the runway, where flooding is modelled to occur as a result of flow exceeding the tunnel's conveyance capacity. Instead of using discharge from the channel at the points on Figure 10 to flood the runway, we use the river, water level and sea-level rise conditions shown in Figure 9 for each tunnel constriction scenario. This allows us to determine the extent to which tunnel constriction at the seawards end of the tunnel increases inundation extent and flood hazard rating of the rear access road.

3 Results

We present the resulting flood extent, depth and hazard rating (methodology in Section 2.1) from each of the model scenarios in a series of maps showing the vulnerability of the runway and the northern RESA (Section 3.1) and the rear access road (Section 3.2). The maps are included as vector graphics, allowing the user to zoom in and out to investigate areas of interests with no loss of image resolution. The co-ordinate system applied to each map is the St Vincent 45/British West Indies Grid (EPSG:2007).

3.1 Runway vulnerability

In this section, we show the inundation extents and flood hazard ratings in the area outlined in white on Figure 12, the main runway and the Runway End Safety Areas (RESA).



Figure 12: Satellite imagery showing the geographic extent of the presented flood maps. ©2018 Google.

We compare the flood extent with the minimum width required for the northern RESA to comply with International Civil Aviation Organisation regulations (90 m, double the established width of the runway). Flood waters reducing the effective width of the RESA may present operational problems for the airport, as the RESA is required to provide a safety barrier for aircraft which either fail to take off, or incorrectly approach the runway. We present the RESA threshold as a black dashed line on flood (Figure 13) and hazard (Figure 14) outputs to see whether the inundation extent could prohibit the RESA from meeting operational requirements. Due to inundation extents and hazard ratings being similar across the scenarios, we only present the worst cases in each sea-level rise scenario, which is 100% tunnel constriction and the 1:50 yr design hydrograph. Figures for the other scenarios can be found in Appendix A.

The modelling shows that overspill into the runway area (white outline, Figure 12) under each sea-level rise scenario occurs as following:

1. Present-day: Under tunnel constrictions of 80% and 100%, regardless of the applied hydrograph.
2. 2100: Under tunnel constrictions of 80% and 100%, regardless of the applied hydrograph.
3. 2500: Regardless of tunnel condition or applied hydrograph. In addition,

sea water overwashing the northern defences also contributes flood water into the area.

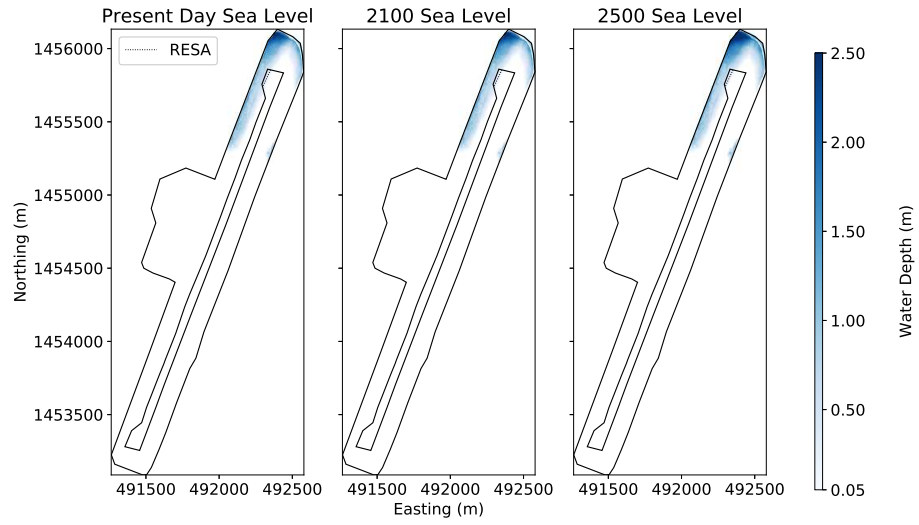


Figure 13: Inundation extents under 100% tunnel constriction with Hydrograph 2 applied for each sea-level scenario.

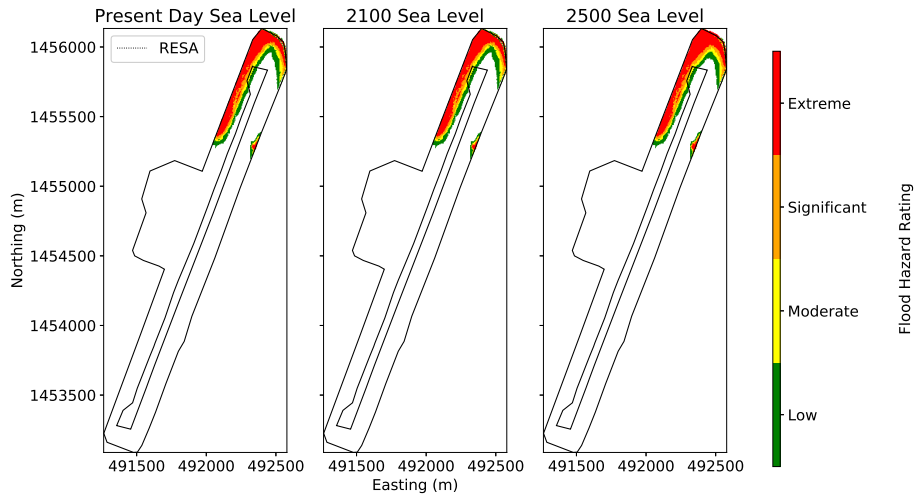


Figure 14: Flood hazard ratings under 100% tunnel constriction with Hydrograph 2 applied for each sea-level scenario.

Figures 13 and 14 show a negligible difference in inundation extent and flood hazard rating on the RESA between sea-level scenarios. This shows the threat to the RESA and the main runway, at least under the present-day and 2100 sea-level scenarios is likely to be derived from River Yambou flood waters. Comparison of Hydrographs 1 and 2 shows a difference of <0.05 m for the majority of grid cells, which is less than the vertical accuracy of the applied DEM. There is no change in flood extent between the two applied hydrographs, Hydrograph 2 delivers a greater volume into the area of concern, however the drainage acts to limit the inundation extent.

Under the 2500 sea-level scenario, some flooding of the area at the northern end of the runway is likely regardless of the performance of the tunnels, due to the magnitude of sea-level rise superimposed on the storm tide. The runway is not inundated under flow constrictions of up to and including 60%, however there is some overspill regardless of the applied flow constriction. Even given the additional flood volume from the northern end of the area, the drainage still performs well to limit the extent of inundation on the runway.

Under all scenarios with flow constrictions of $\geq 80\%$ ($\geq 60\%$ under the 2500 sea-level rise scenario), it is possible that the inundation may act to reduce the width of the RESA below that demanded by operational requirements.

3.2 Access road vulnerability

The inclusion of vegetation and other surface features in the DEM is likely to prevent flood waters propagating across terrain it would otherwise be able to. We therefore show only flood depth and hazard rating in the model grid cells which contain the rear access road.

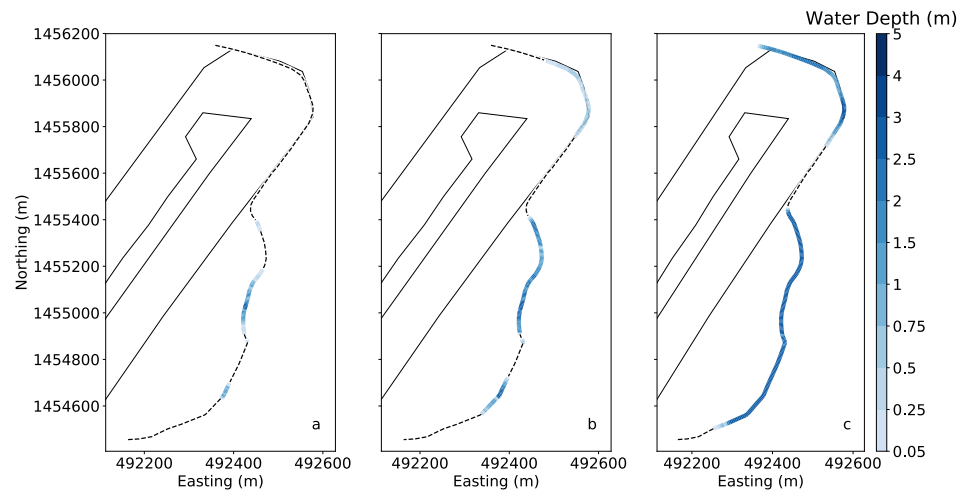


Figure 15: Extent of flooding on the rear access road (black dashed line) with Hydrograph 2 and no tunnel constriction applied for a) present-day sea-level, b) 2100 sea-level (+ 1.10 m), and c) 2500 sea-level (+ 5.48 m).

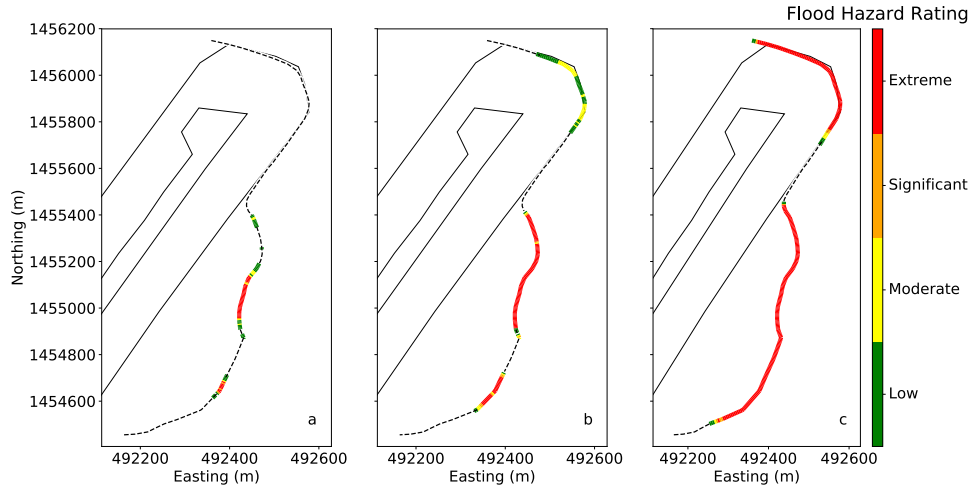


Figure 16: Flood Hazard Rating on the rear access road (black dashed line) with Hydrograph 2 and no tunnel constriction applied for a) present-day sea level, b) 2100 sea level (+ 1.10 m), and c) 2500 sea level (+ 5.48 m).

Approximately 410 m of the access road is shown to be flooded to an extreme flood hazard rating, under a water level representative of Hurricane Ivan, and present-day sea level. The length of the road that is inundated increases to approximately 1075 m, and 1565 m under the 2100 and 2500 sea-level scenarios, respectively. An extreme flood hazard rating would prohibit all road access. The inundation of the access road is shown to mostly be a function of the water level and sea-level rise scenario. The tunnel constriction and the river flow are shown to have a negligible impact on the overall inundation extent. Accordingly, we only present results for each sea-level scenario, where the tunnels are unconstricted, and Hydrograph 2 is applied. Flood extent and hazard rating outputs for the other scenarios can be found in Appendix B.

4 Conclusions and recommendations

These results cannot be taken as a prediction of a future inundation event. Rather, they demonstrate the impact of coarse sediment deposition in the northernmost tunnels on inundation extent based on design events derived from modelled data. Although failure or non-failure of the tunnels is not shown to be dependent on the design hydrographs, a lack of river flow data and sub-daily precipitation data introduces large uncertainty in determining the watershed response to extreme rainfall events, and the resulting flood hazard. The conceptu-

alisation of the tunnel where the applied model does not resolve incompressible tunnel flow also contributes to the uncertainty in the findings.

The key findings based on the applied approach are as follows:

1. The northern Runway End Safety Area is shown to be partially inundated under tunnel constrictions of 80-100% under present-day and 2100 sea-level scenarios, and 60% - 100% for the 2500 sea-level scenario. This reduces the margin of error for aircraft which incorrectly approach or have an aborted take off and is likely to reduce the ease of access for emergency services. With the effective width of the RESA reduced due to inundation, it may not comply with regulations which state that for a Code 4 runway, the width of the RESA should be a minimum of twice the width of the defined runway (90 m). The main runway is not shown to be flooded under any of the applied scenarios.
2. The rear access road is shown to be vulnerable to inundation, under present-day sea level and regardless of the condition of the tunnels. Flood extents and hazard ratings are shown to be similar under 1.1 m sea-level rise, with large increases in the length of road flooded in the 2500 sea-level rise scenario. Given the low elevation of certain parts of the access road, the flood hazard rating is shown to be extreme, which is likely to prohibit access even under present-day sea-level.

Efforts to collect observational data should focus on collecting high temporal resolution rainfall data, with ideally rainfall intensity measured every minute, as in St Lucia. Monitoring of the River Yambou during extreme events would be unlikely to provide accurate data given the probability of instruments being damaged, but some observational data under less extreme conditions would be required to validate the rainfall-runoff model. Whilst there is large uncertainty in the applied approach it shows the importance of regularly excavating the river channel at the outflow in order to alleviate flow constriction.

This work provides a worked example of using freely available models to account for multi-modal flooding from coastal and riverine sources, which could be used in future flood risk assessments should more observational data become available to improve confidence in the outputs.

5 Acknowledgements

This work was funded by a U.K. Research & Innovation Global Challenges Research Fund Impact Acceleration Award. David Byrne and Michela de Dominicis (National Oceanography Centre) are acknowledged for provision of the modelled water level and wave boundary conditions. We also acknowledge the U.K. Hydrographic Office for providing the multibeam LiDAR bathymetric survey.

A Runway flood maps

Herein are the runway inundation figures not presented in Section 3.1, due to inundation extents and hazard ratings being similar across scenarios.

Present Day Sea Level

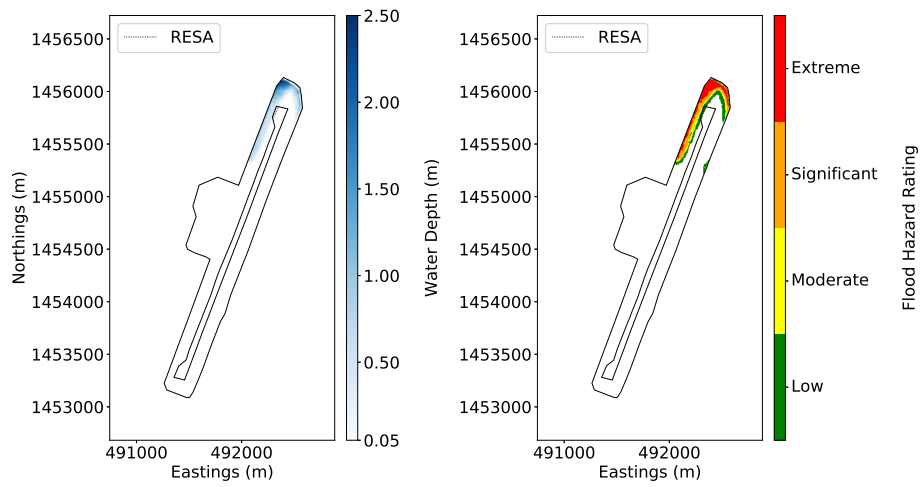


Figure A1: Hydrograph 1, present-day sea level, tunnel flow constricted by 80%.

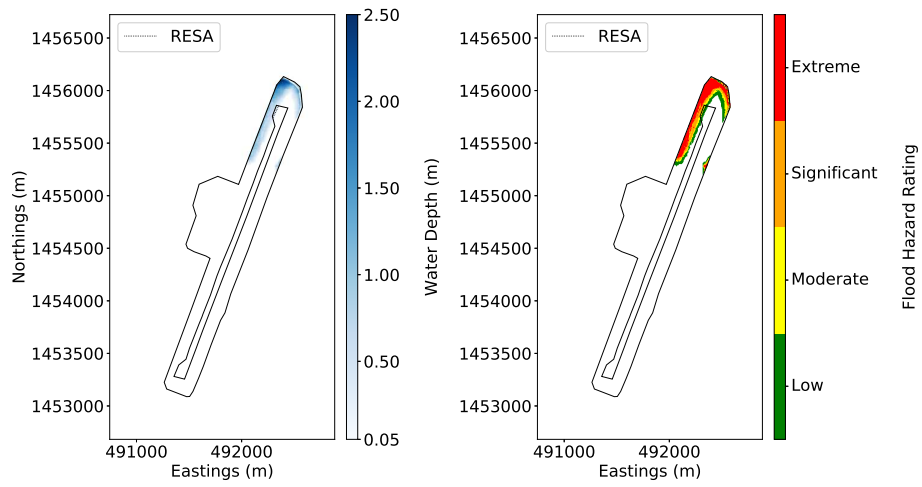


Figure A2: Hydrograph 1, present-day sea level, tunnel flow constricted by 100%.

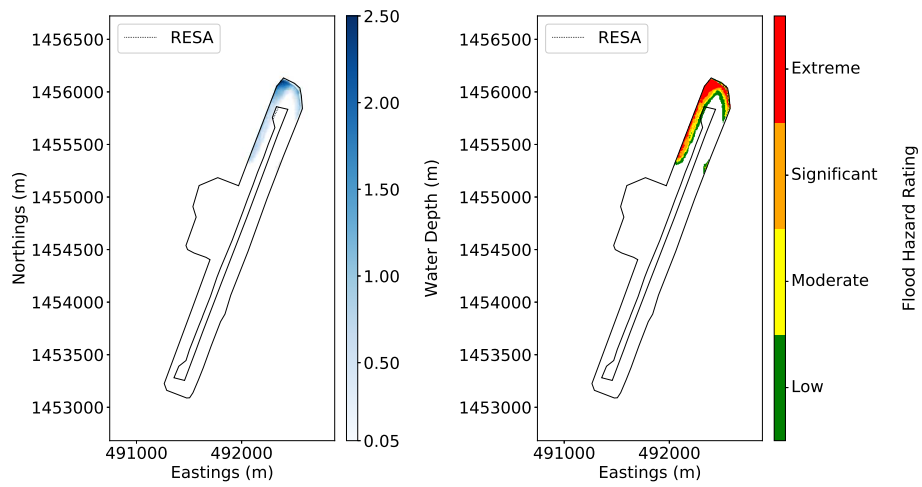


Figure A3: Hydrograph 1, present-day sea level, tunnel flow constricted by 80%.

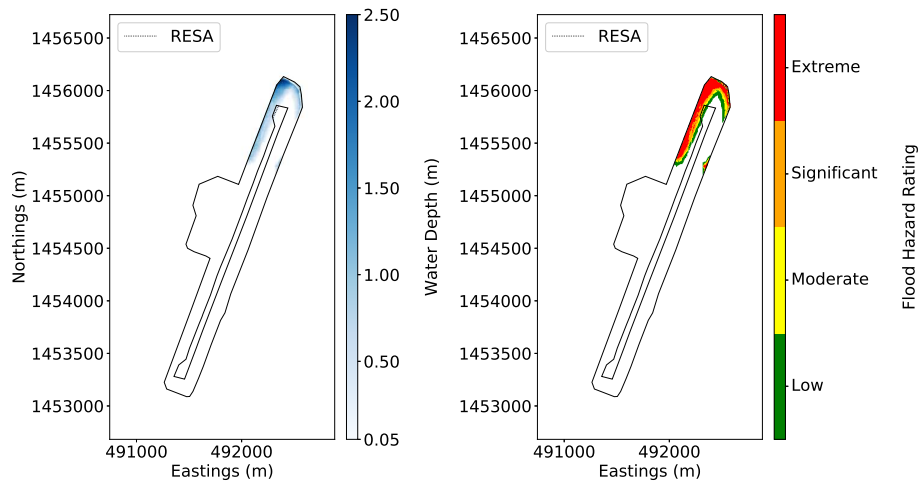


Figure A4: Hydrograph 1, present-day sea level, tunnel flow constricted by 100%.

2100 Sea Level

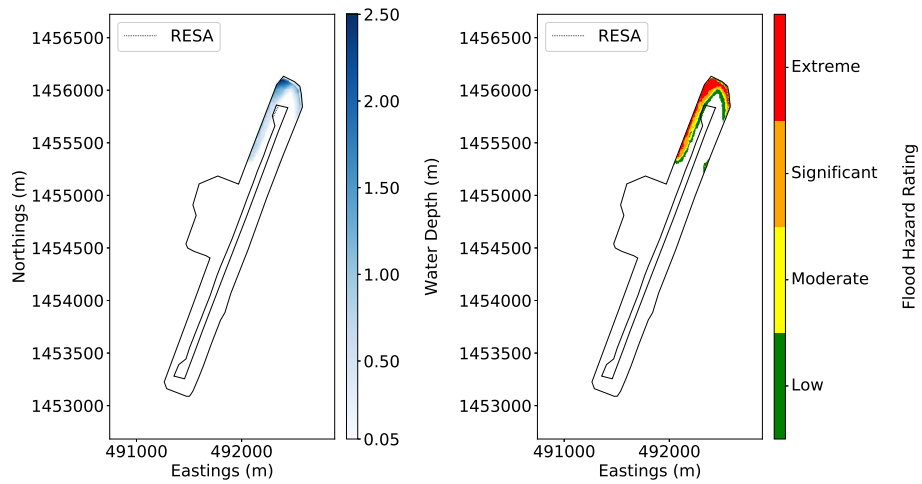


Figure A5: Hydrograph 1, 2100 sea level, tunnel flow constricted by 80%.

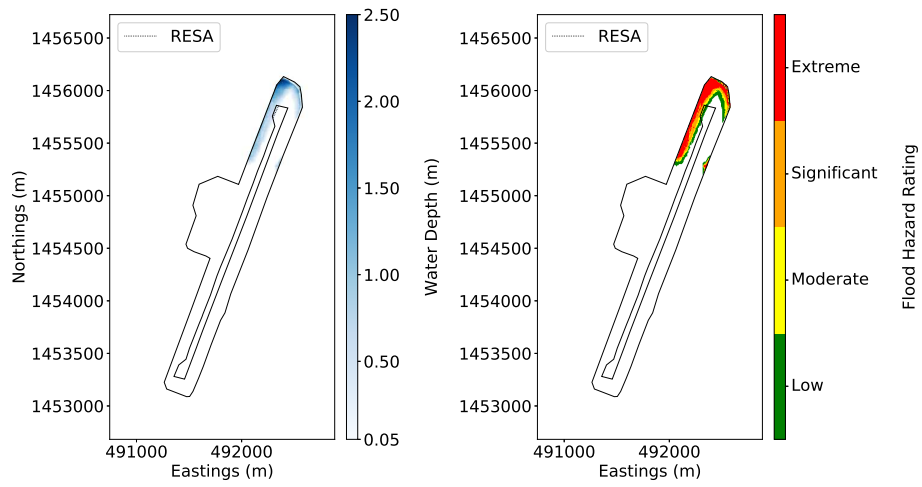


Figure A6: Hydrograph 1, 2100 sea level, tunnel flow constricted by 100%.

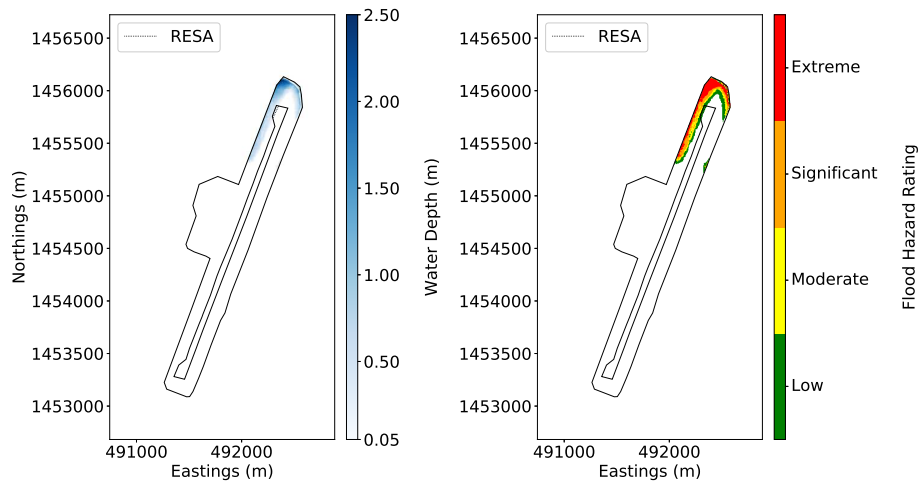


Figure A7: Hydrograph 2, 2100 sea level, tunnel flow constricted by 80%.

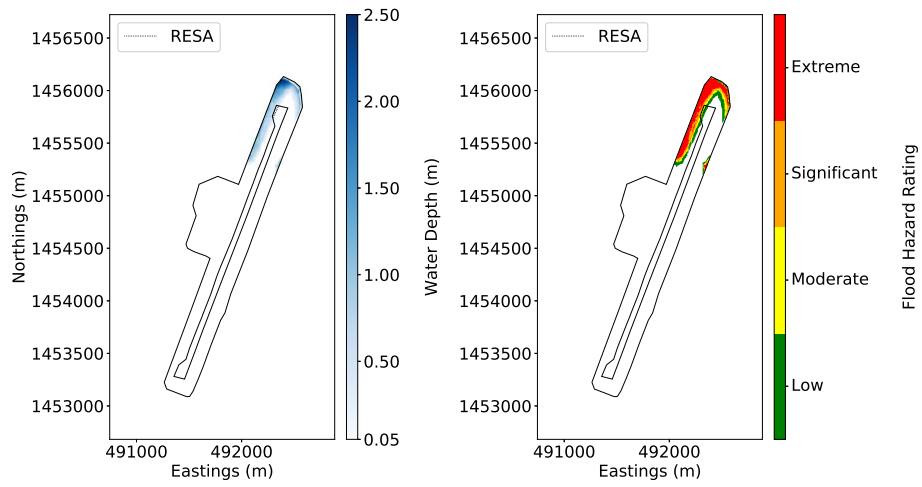


Figure A8: Hydrograph 2, 2100 sea level, tunnel flow constricted by 100%.

2500 Sea Level

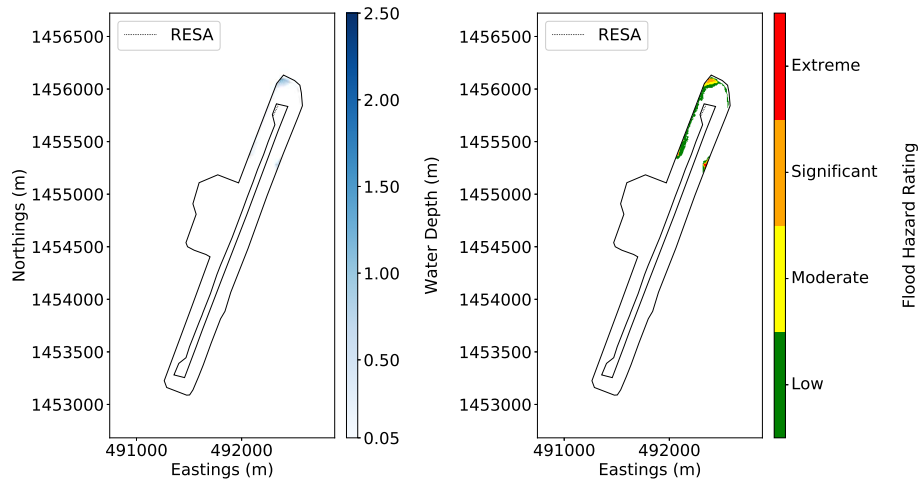


Figure A9: Hydrograph 1, 2500 sea level, tunnel flow constricted by 20%.

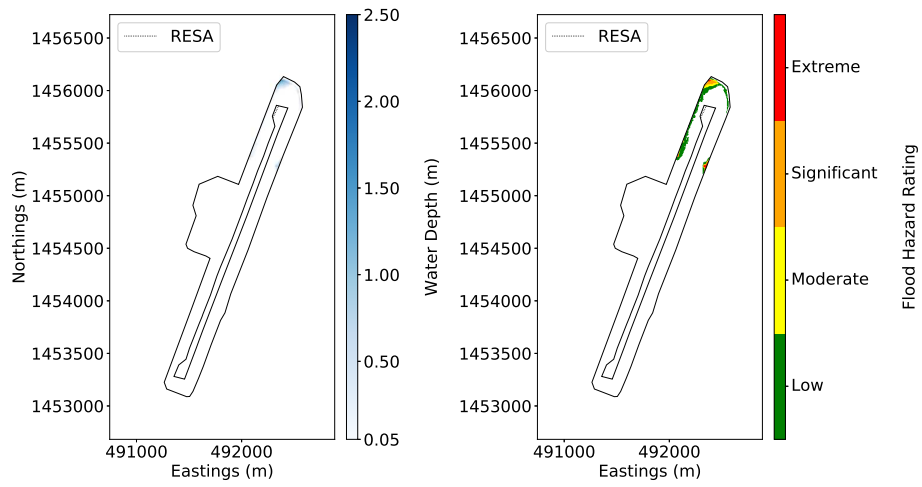


Figure A10: Hydrograph 1, 2500 sea level, tunnel flow constricted by 40%.

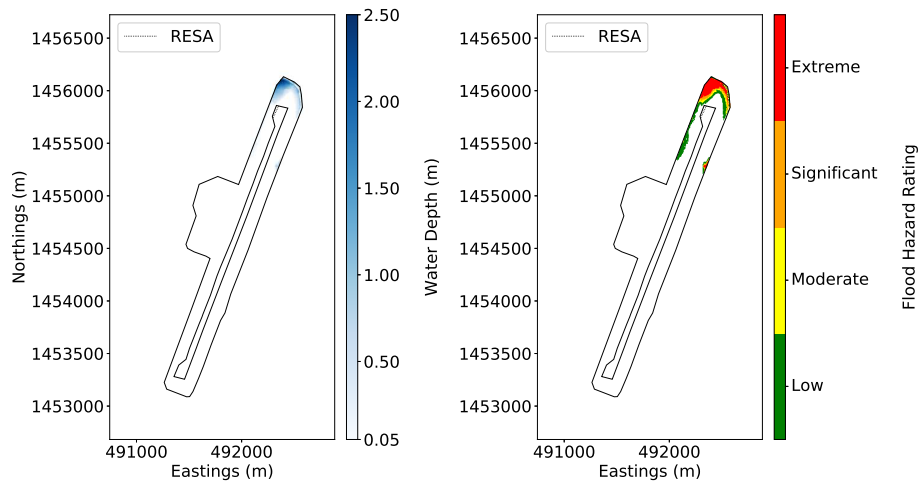


Figure A11: Hydrograph 1, 2500 sea level, tunnel flow constricted by 60%.

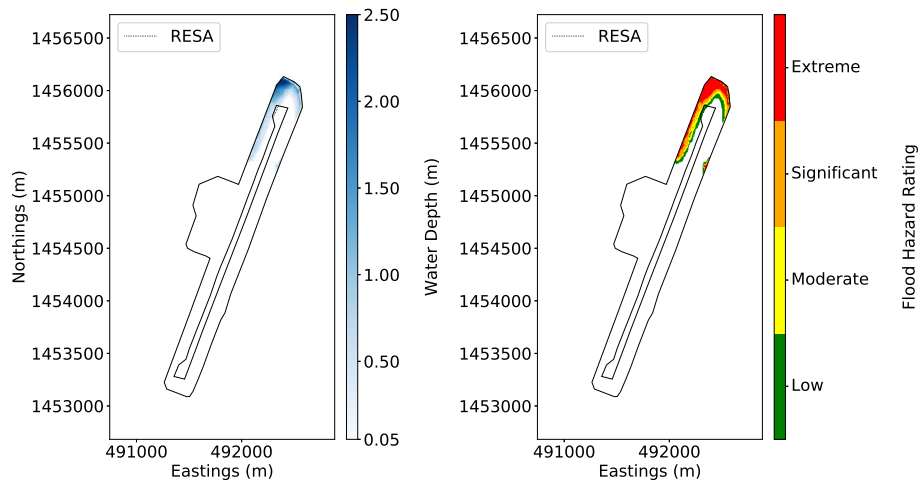


Figure A12: Hydrograph 1, 2500 sea level, tunnel flow constricted by 80%.

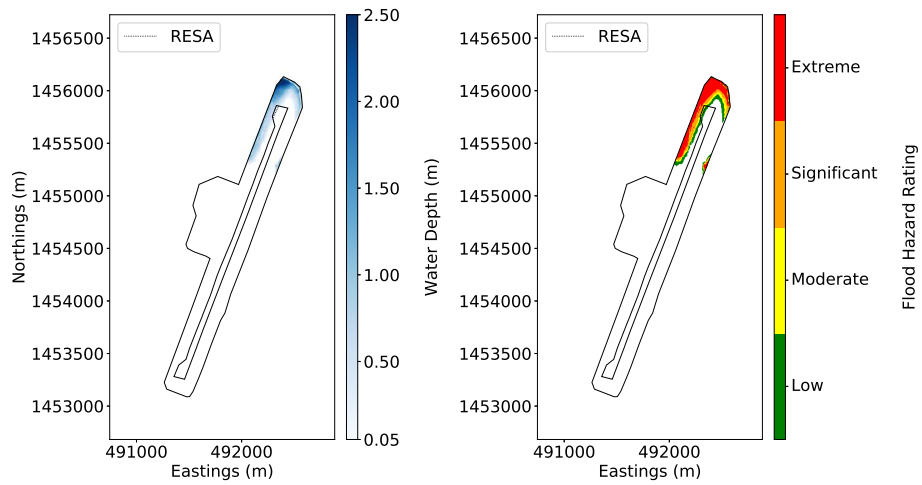


Figure A13: Hydrograph 1, 2500 sea level, tunnel flow constricted by 100%.

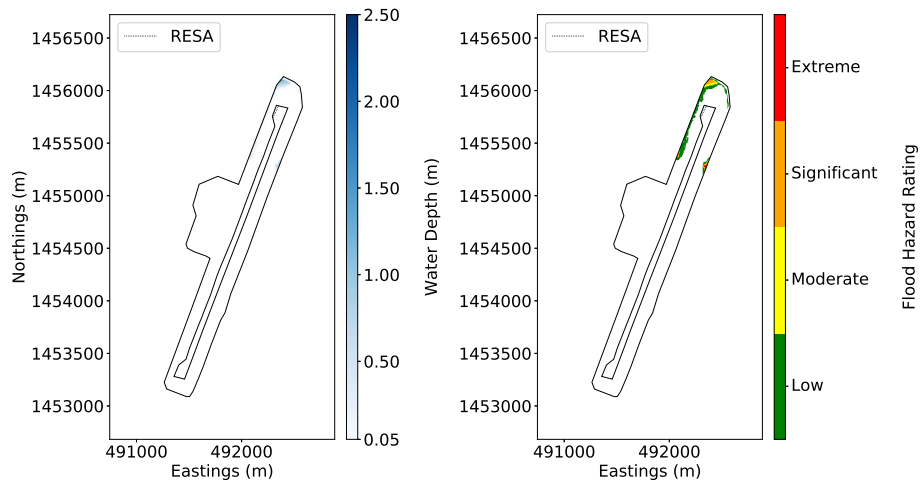


Figure A14: Hydrograph 2, 2500 sea level, tunnel flow constricted by 20%.

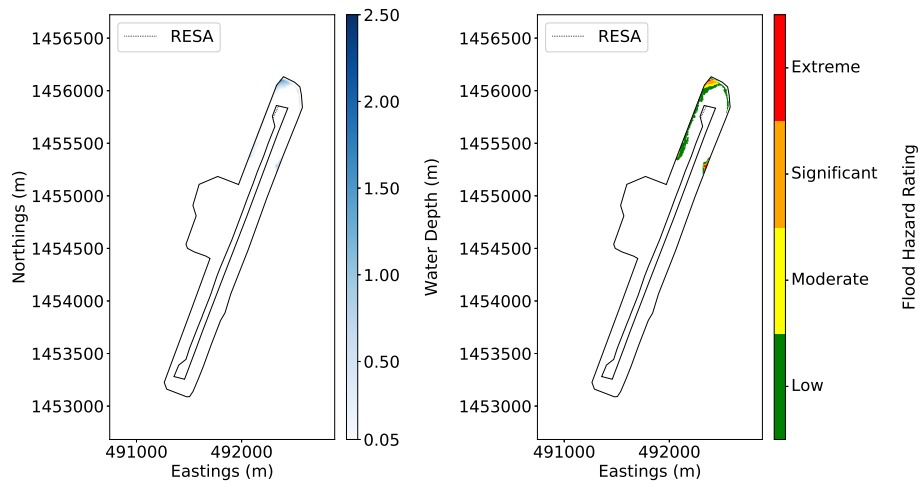


Figure A15: Hydrograph 2, 2500 sea level, tunnel flow constricted by 40%.

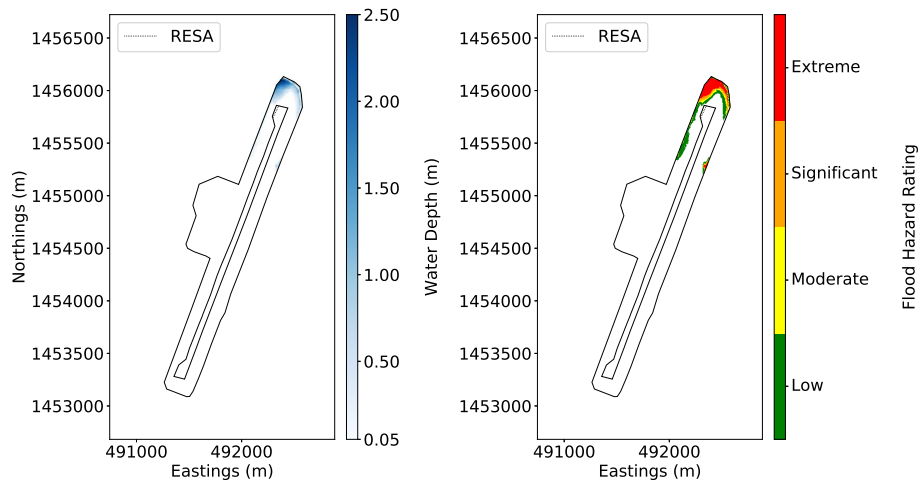


Figure A16: Hydrograph 2, 2500 sea level, tunnel flow constricted by 60%.

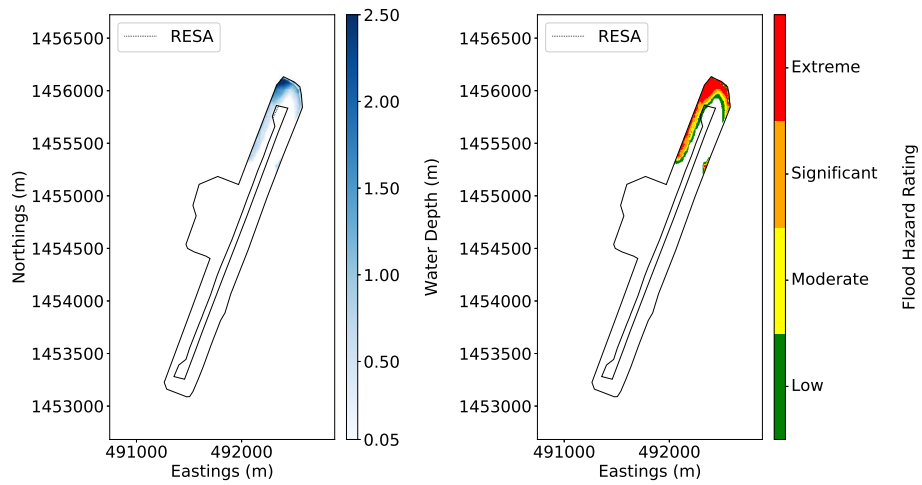


Figure A17: Hydrograph 2, 2500 sea level, tunnel flow constricted by 80%.

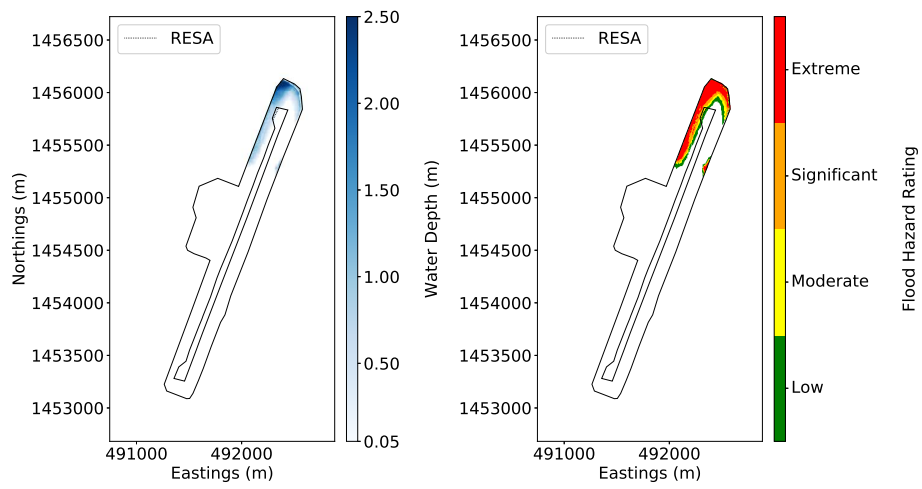


Figure A18: Hydrograph 2, 2500 sea level, tunnel flow constricted by 100%.

B Access road flood maps

Herein are the access road inundation figures not presented in Section 3.2, due to inundation extents and hazard ratings being similar across scenarios.

Present-day Sea Level

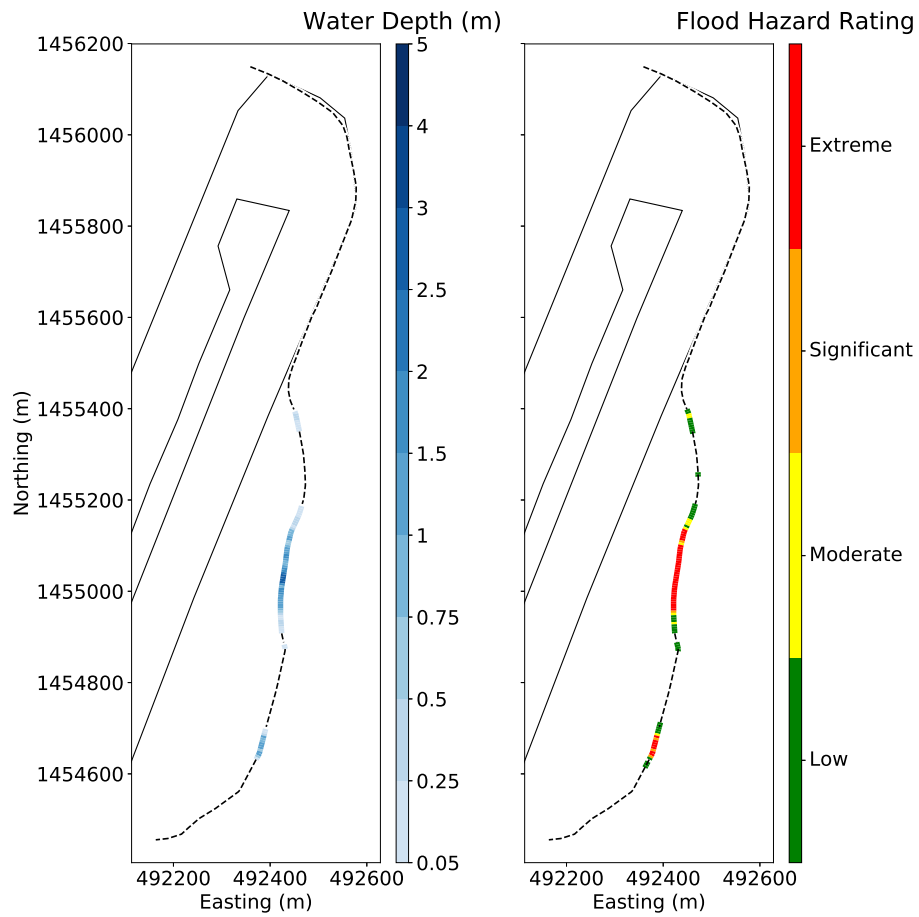


Figure B1: Hydrograph 1, present-day sea level, tunnel flow constricted by 20%.

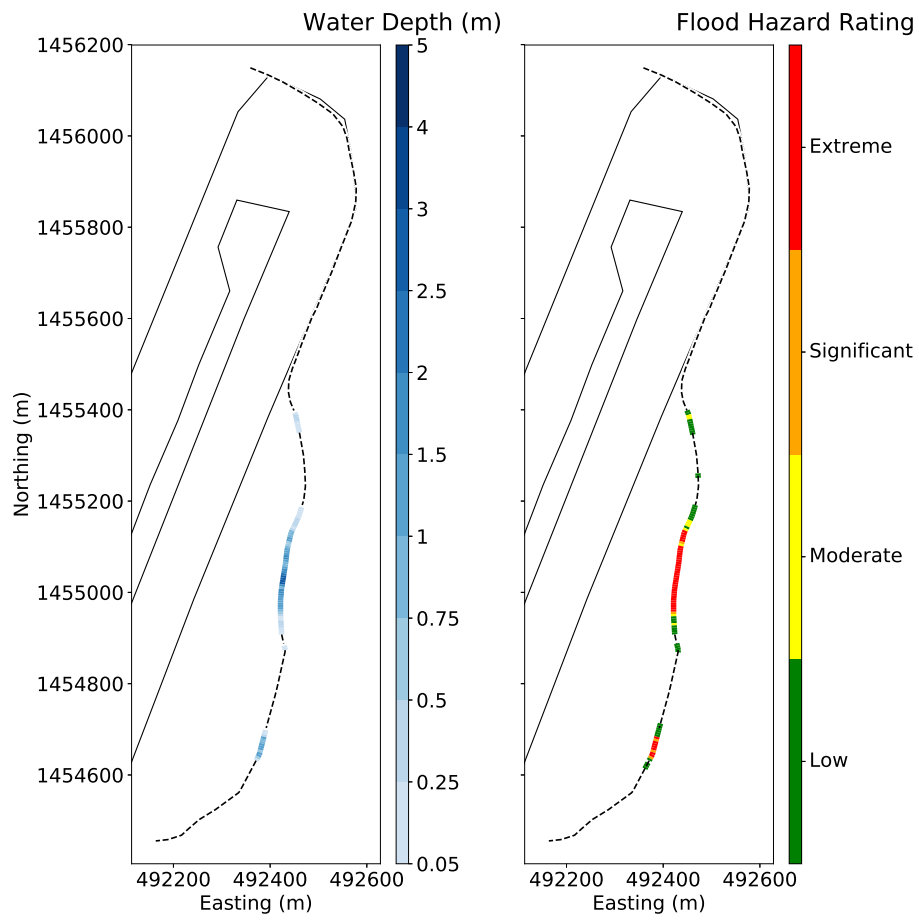


Figure B2: Hydrograph 1, present-day sea level, tunnel flow constricted by 40%.

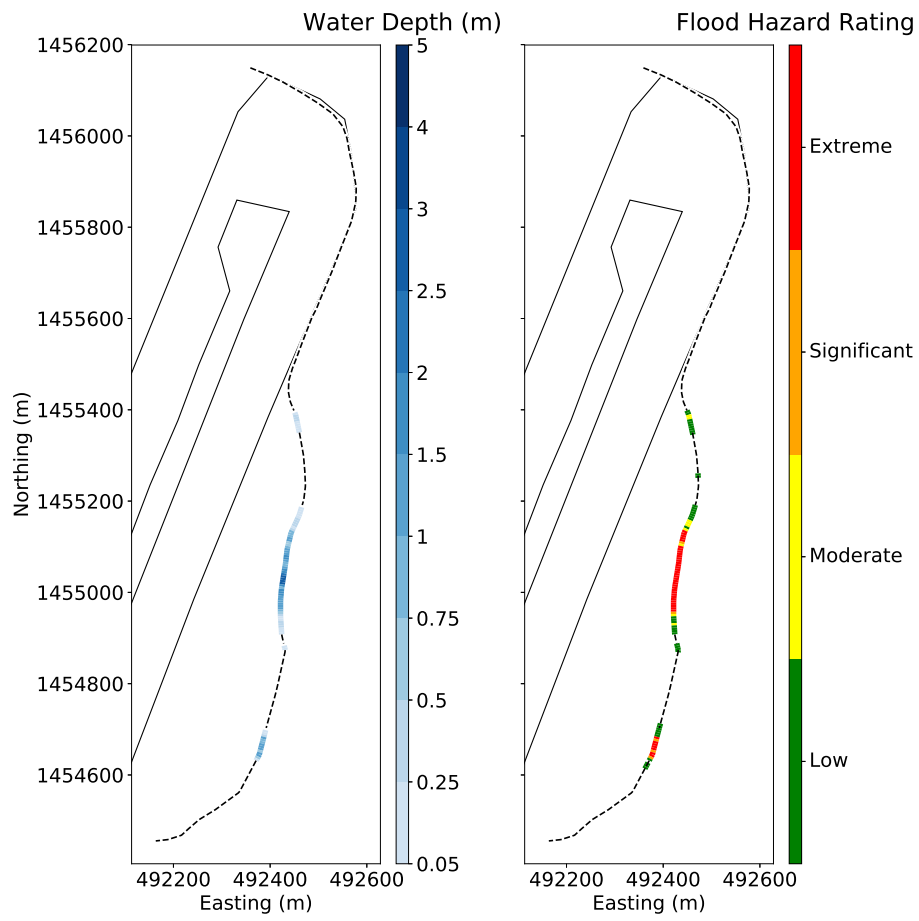


Figure B3: Hydrograph 1, present-day sea level, tunnel flow constricted by 60%.

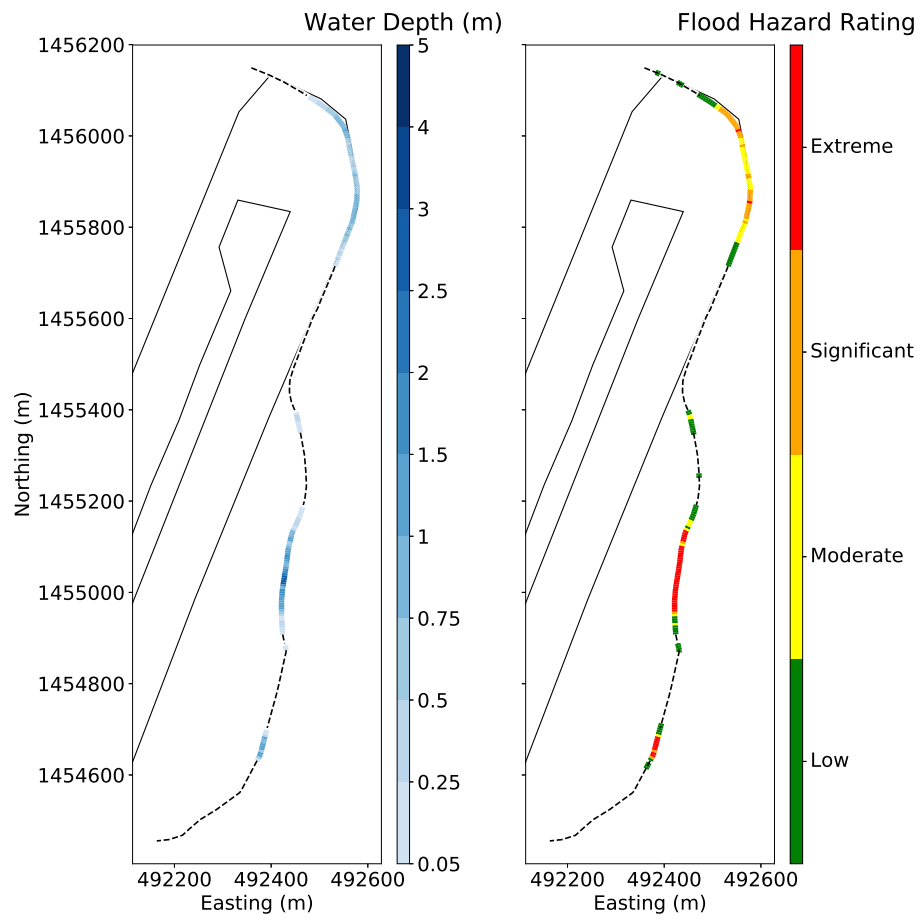


Figure B4: Hydrograph 1, present-day sea level, tunnel flow constricted by 80%.

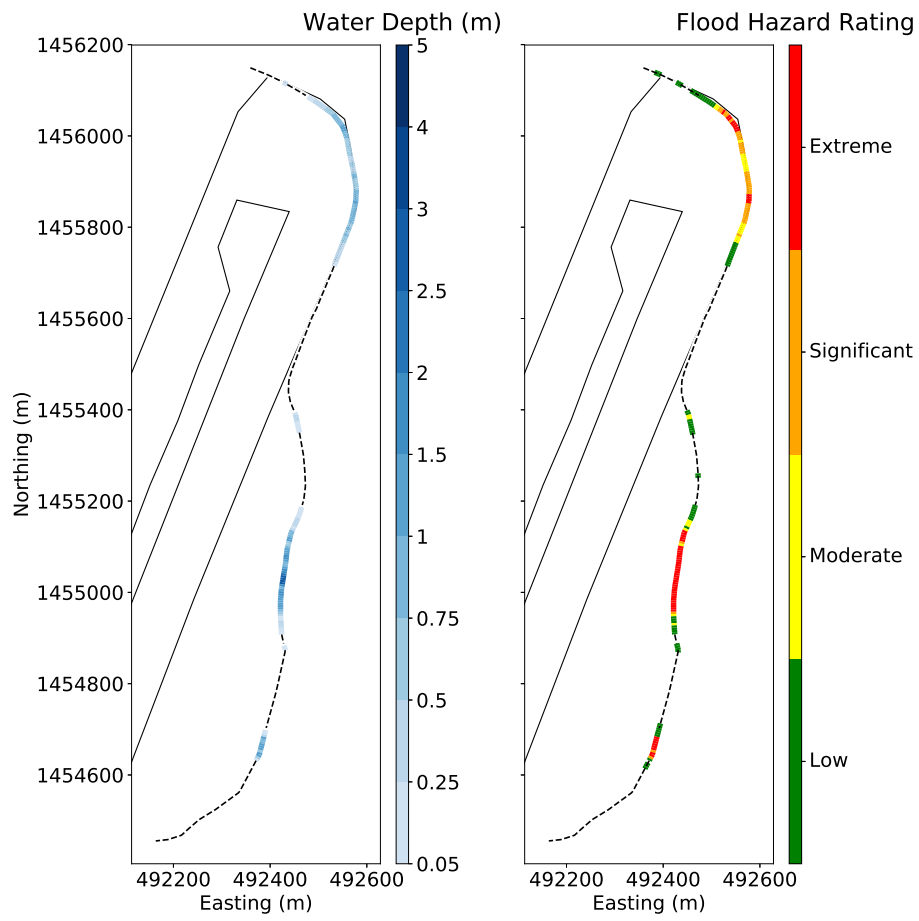


Figure B5: Hydrograph 1, present-day sea level, tunnel flow constricted by 100%.

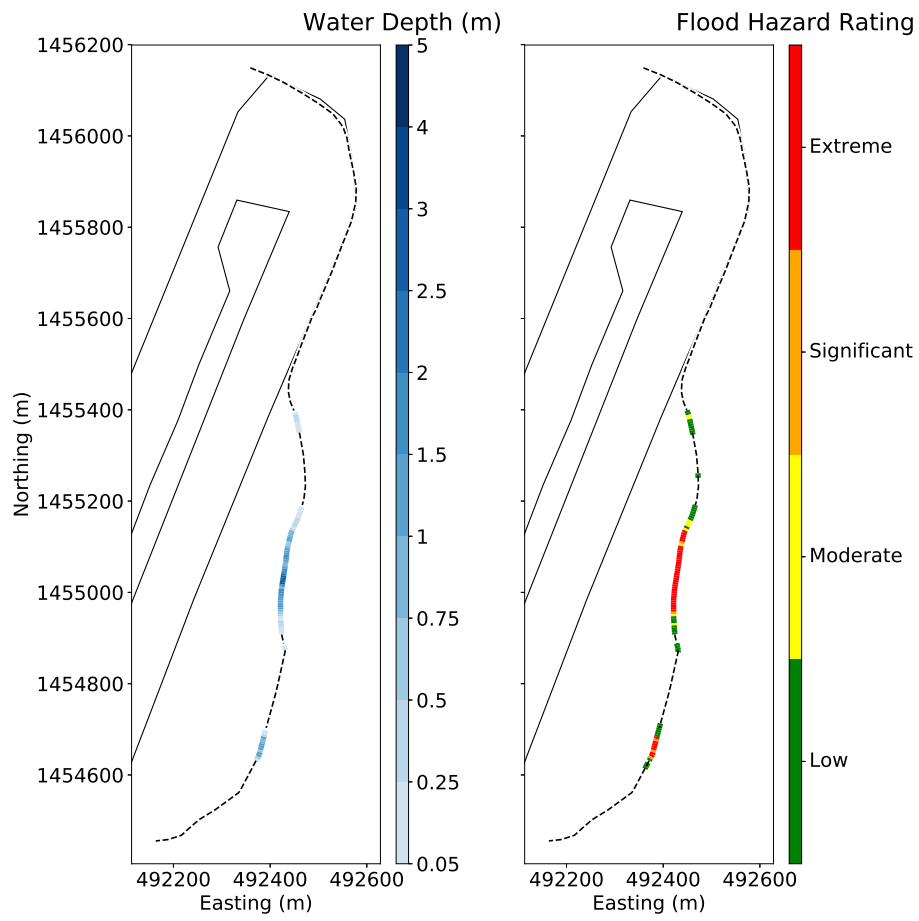


Figure B6: Hydrograph 2, present-day sea level, tunnel flow constricted by 20%.

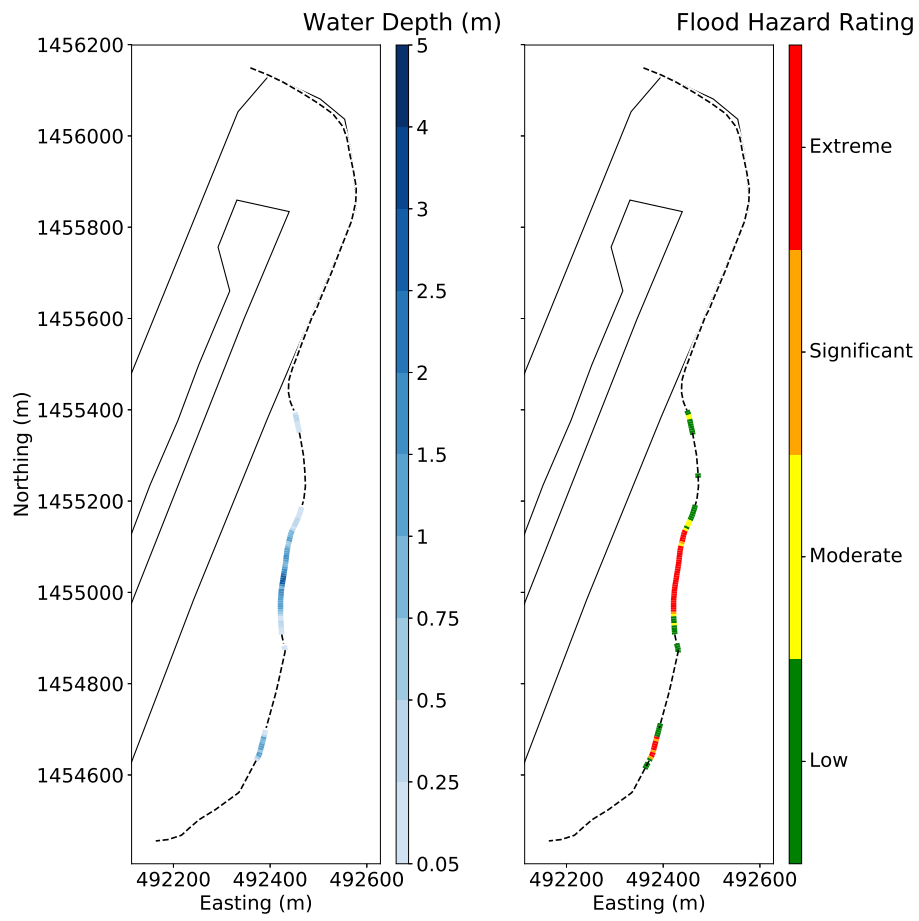


Figure B7: Hydrograph 2, present-day sea level, tunnel flow constricted by 40%.

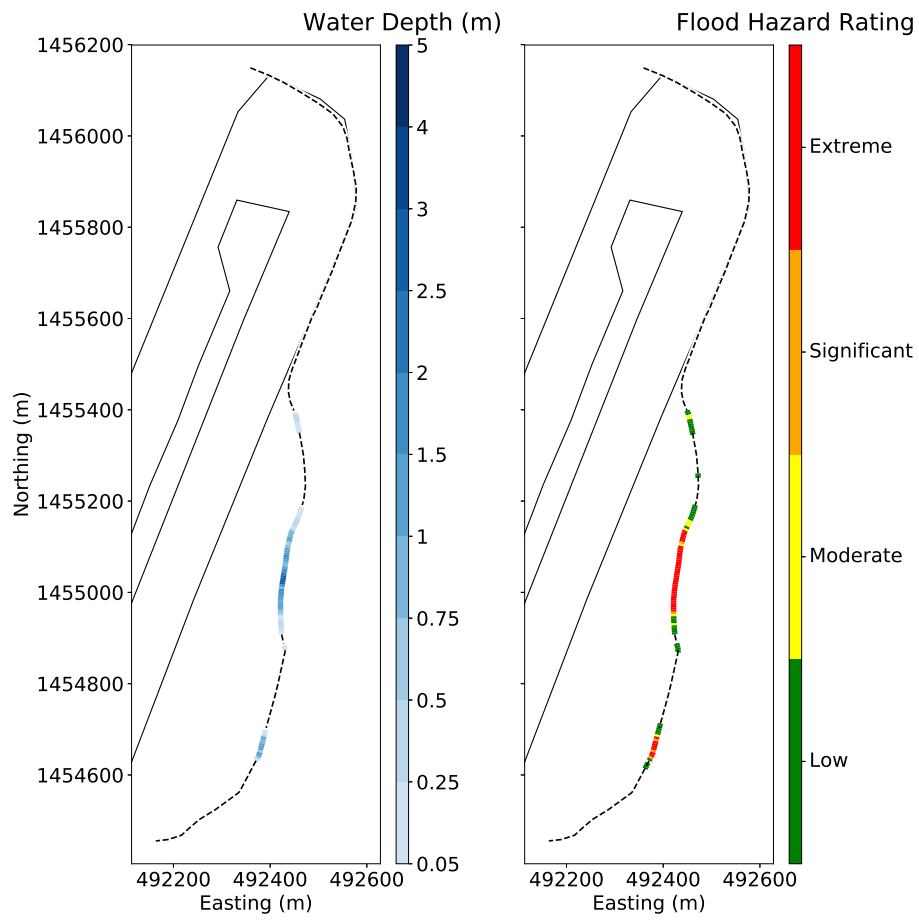


Figure B8: Hydrograph 2, present-day sea level, tunnel flow constricted by 60%.

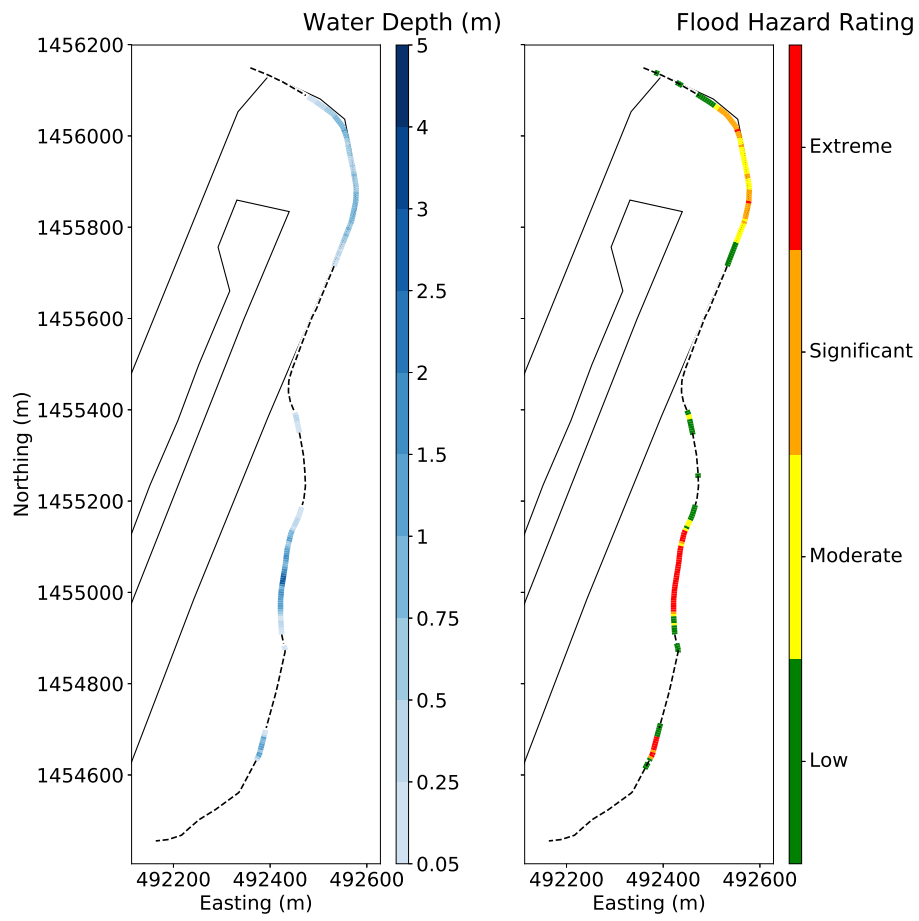


Figure B9: Hydrograph 2, present-day sea level, tunnel flow constricted by 80%.

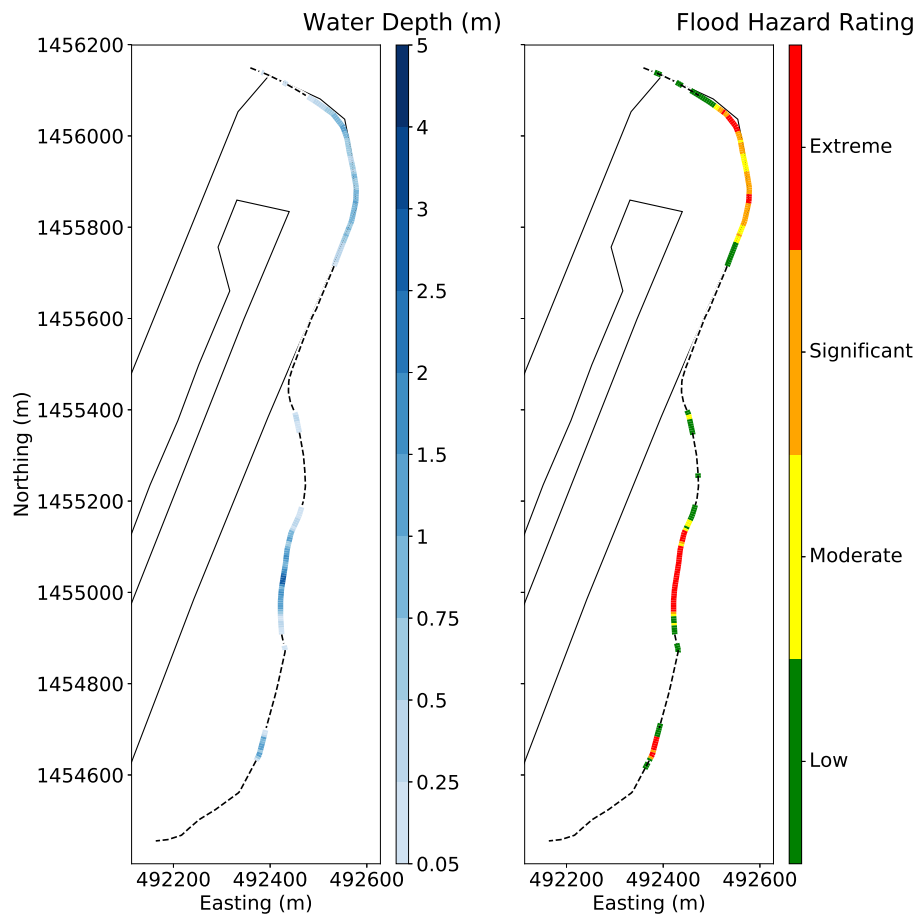


Figure B10: Hydrograph 2, present-day sea level, tunnel flow constricted by 100%.

2100 Sea Level

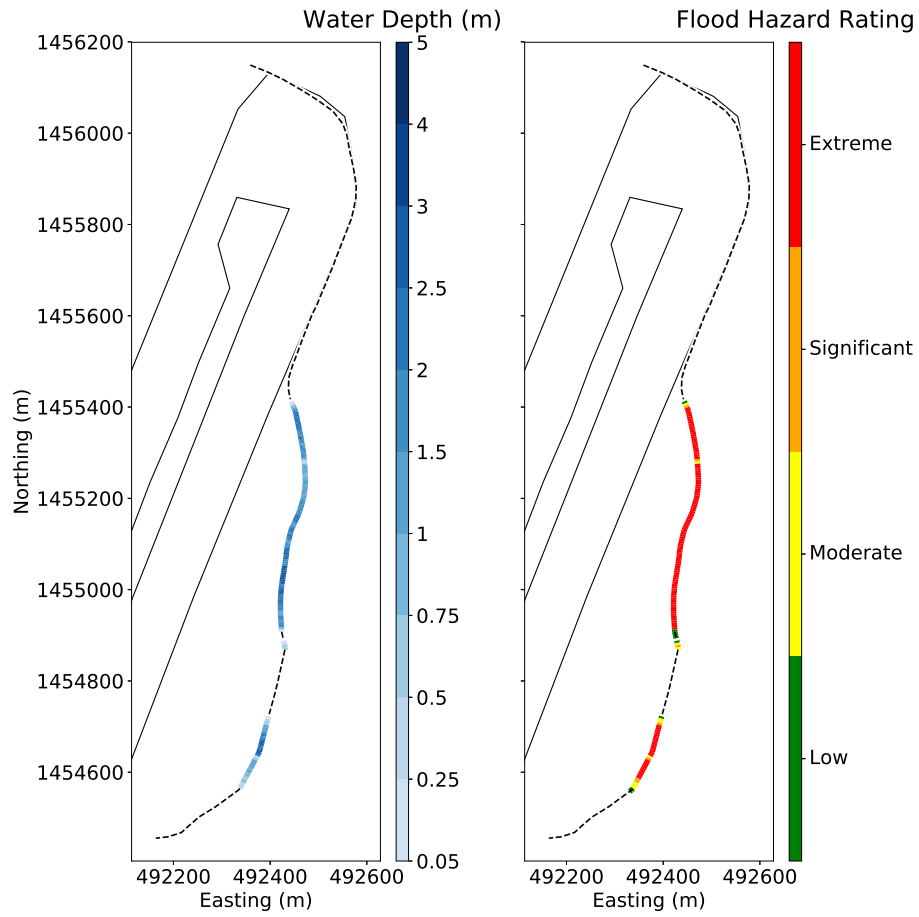


Figure B11: Hydrograph 1, 2100 sea level, tunnel flow constricted by 20%.

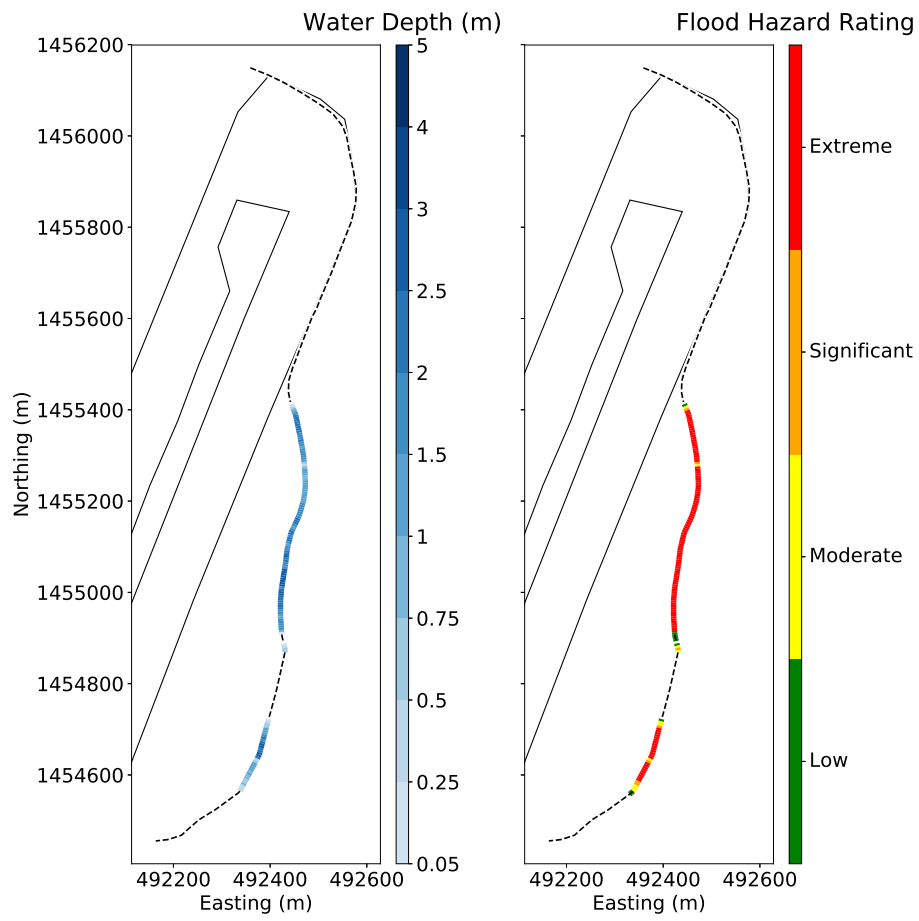


Figure B12: Hydrograph 1, 2100 sea level, tunnel flow constricted by 40%.

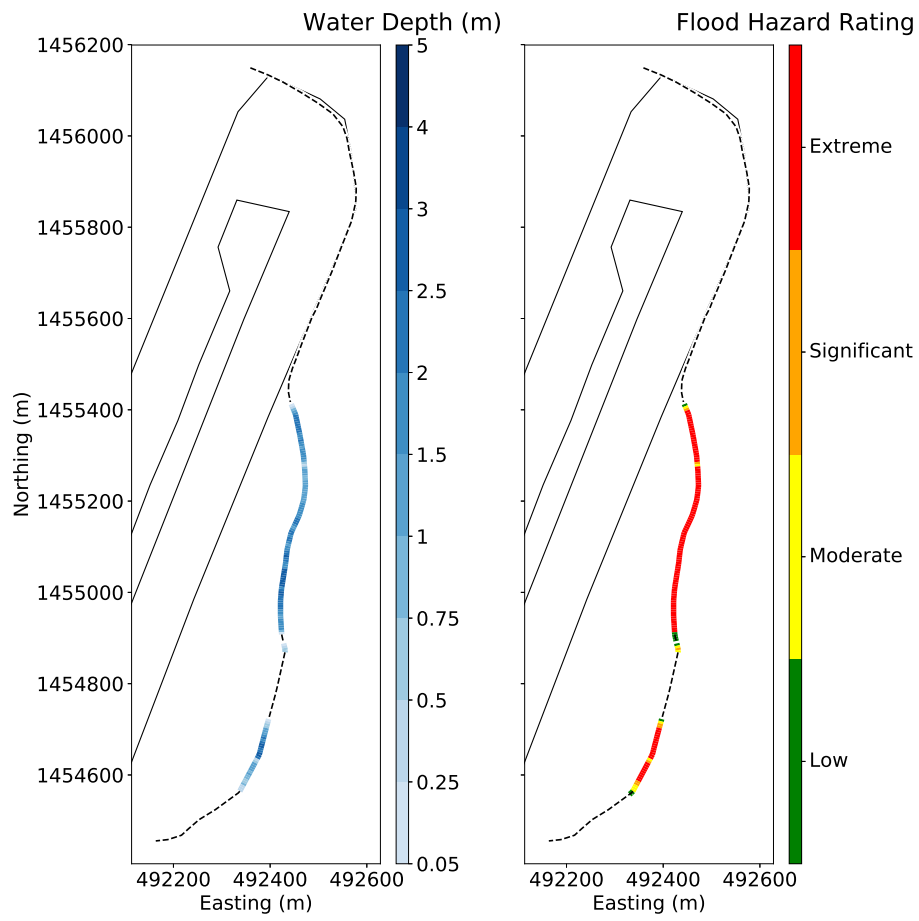


Figure B13: Hydrograph 1, 2100 sea level, tunnel flow constricted by 60%.

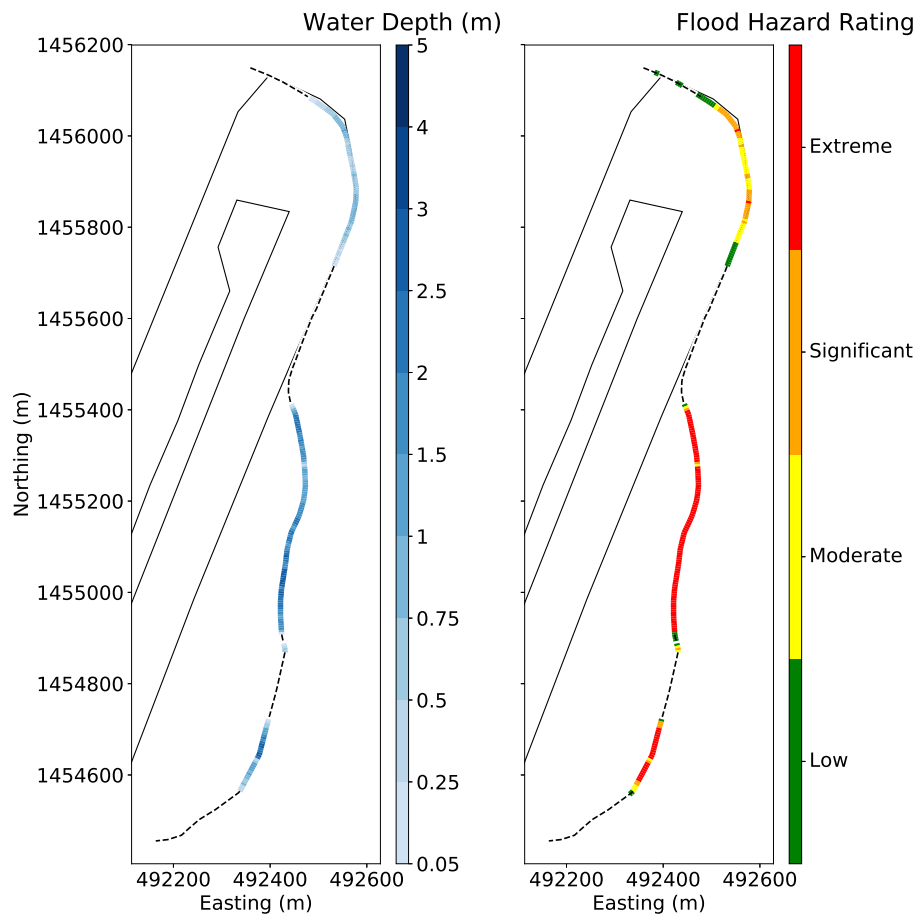


Figure B14: Hydrograph 1, 2100 sea level, tunnel flow constricted by 80%.

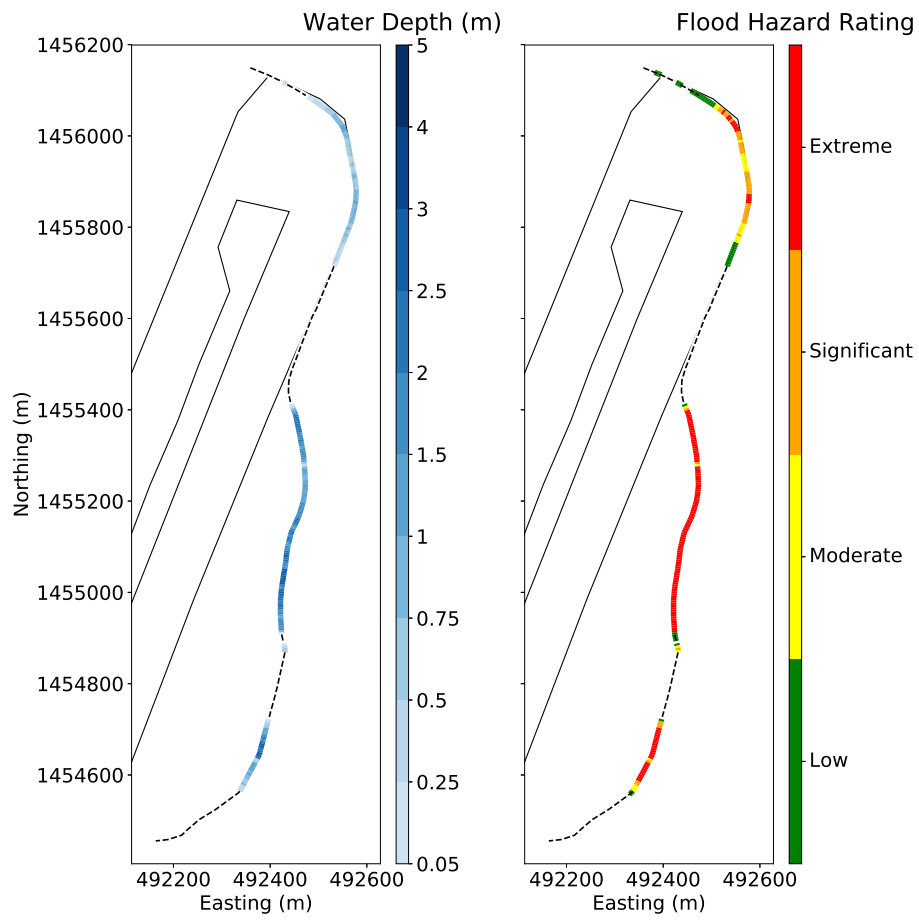


Figure B15: Hydrograph 1, 2100 sea level, tunnel flow constricted by 100%.

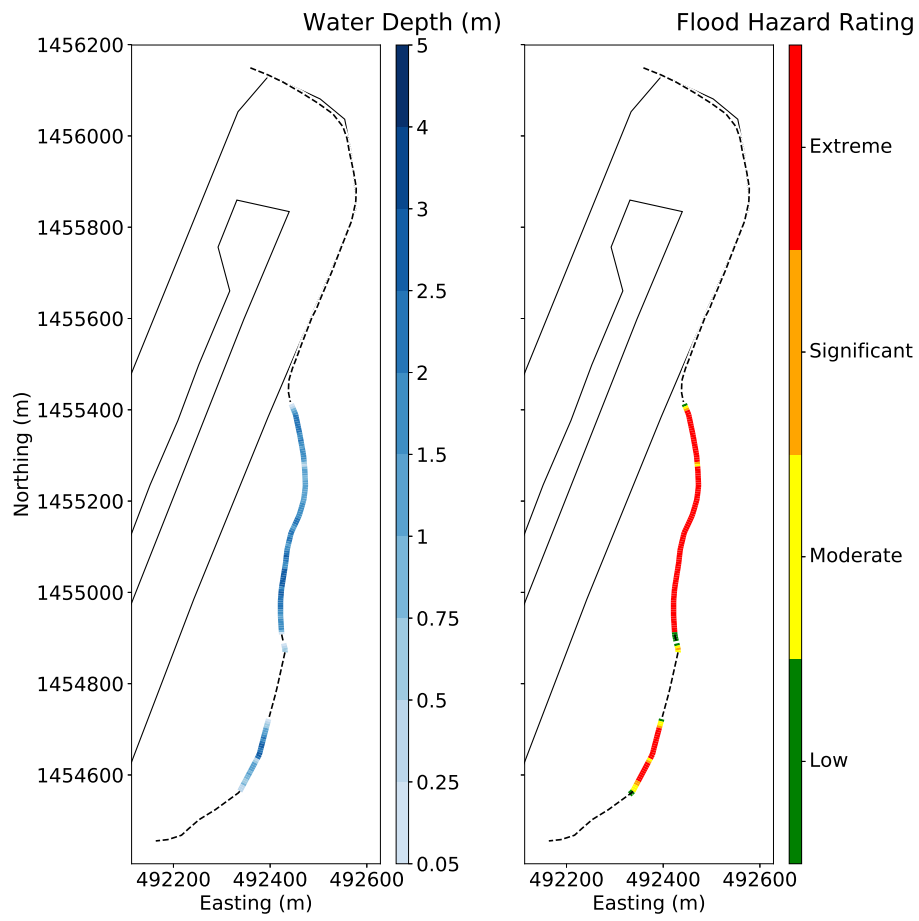


Figure B16: Hydrograph 2, 2100 sea level, tunnel flow constricted by 20%.

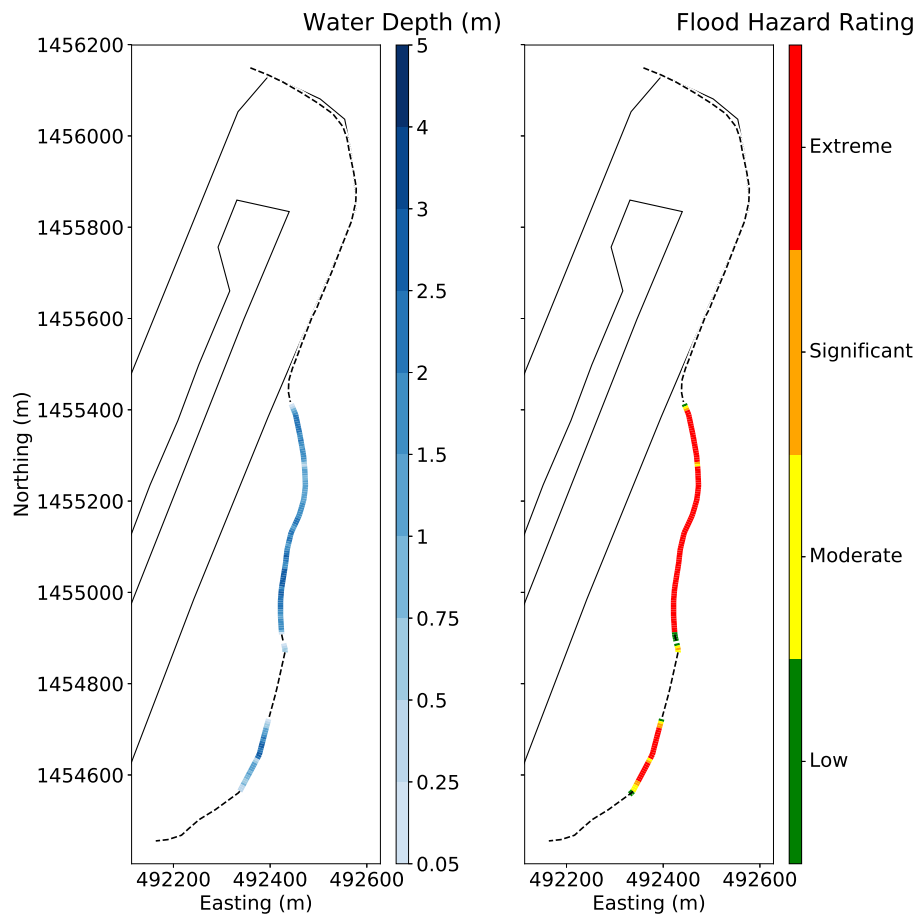


Figure B17: Hydrograph 2, 2100 sea level, tunnel flow constricted by 40%.

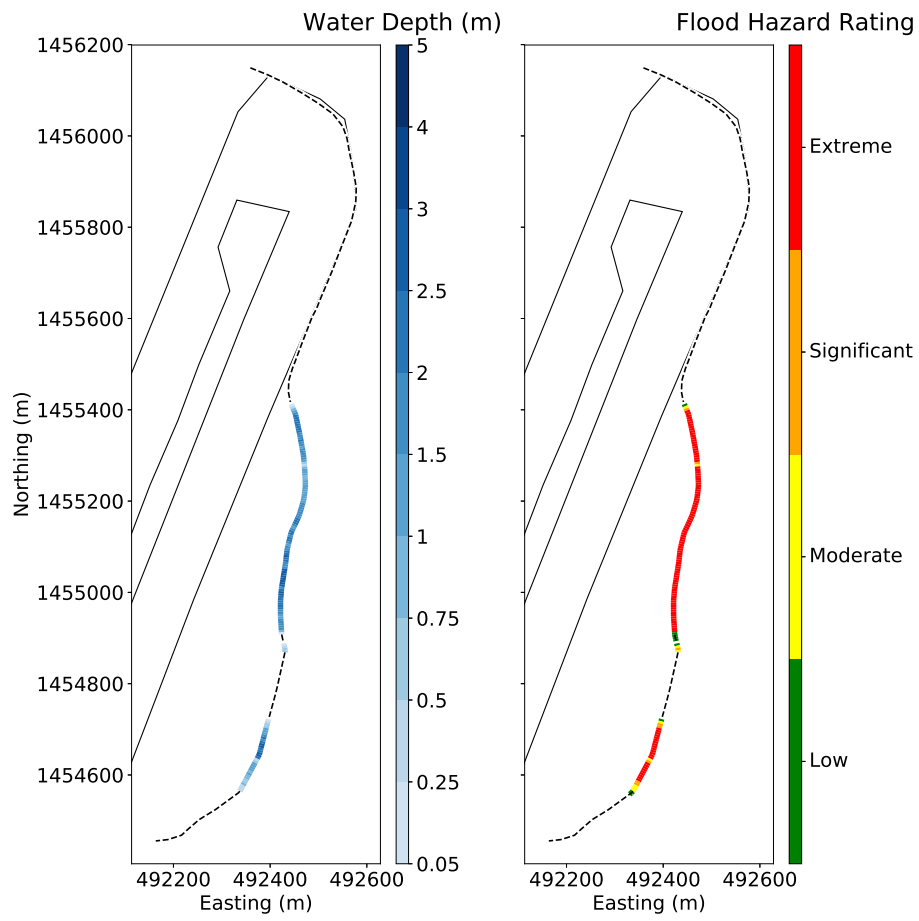


Figure B18: Hydrograph 2, 2100 sea level, tunnel flow constricted by 60%.

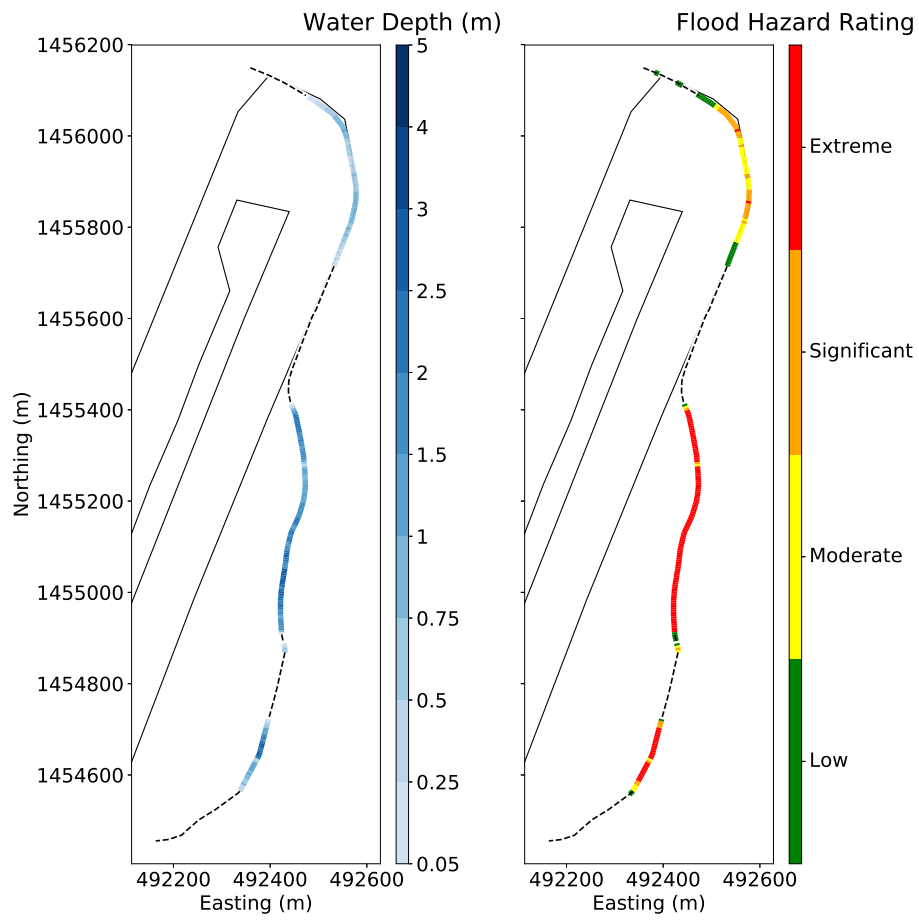


Figure B19: Hydrograph 2, 2100 sea level, tunnel flow constricted by 80%.

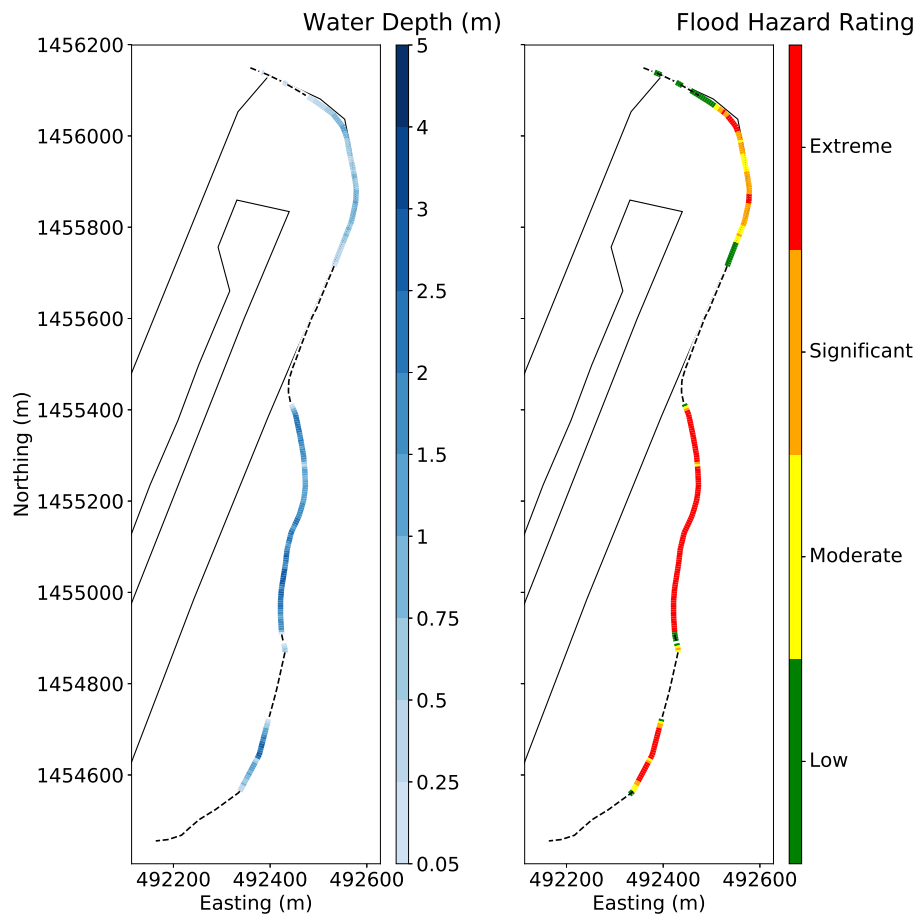


Figure B20: Hydrograph 2, 2100 sea level, tunnel flow constricted by 100%.

2500 Sea Level

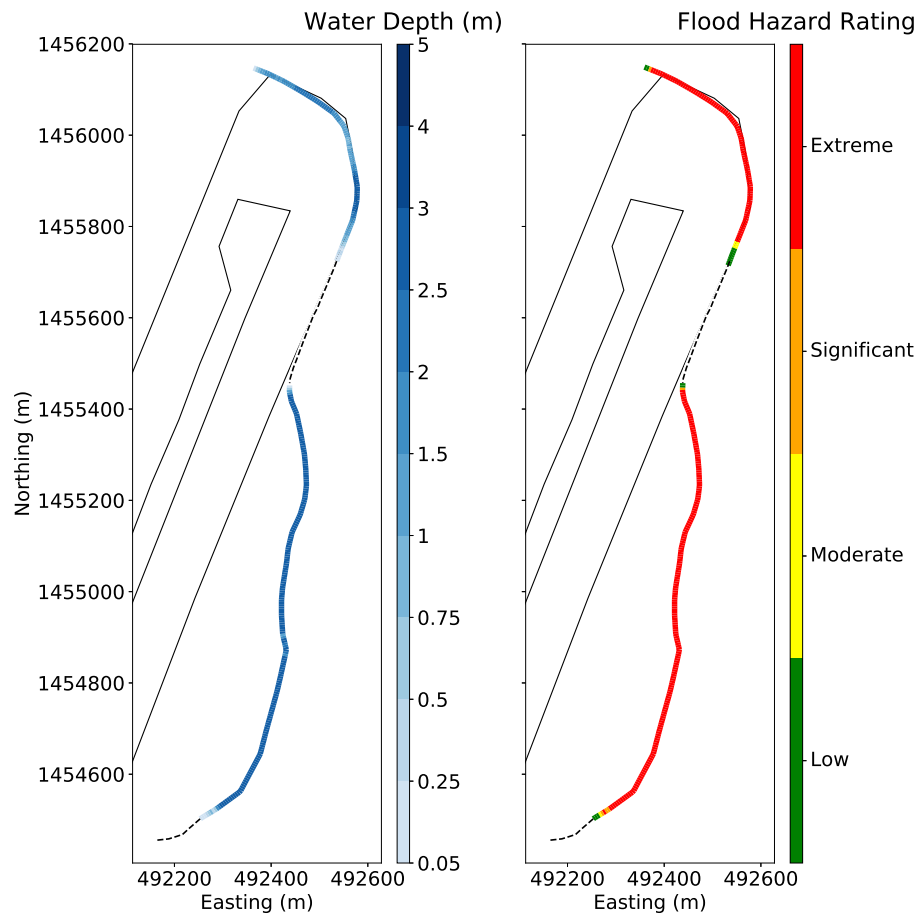


Figure B21: Hydrograph 1, 2500 sea level, tunnel flow constricted by 20%.

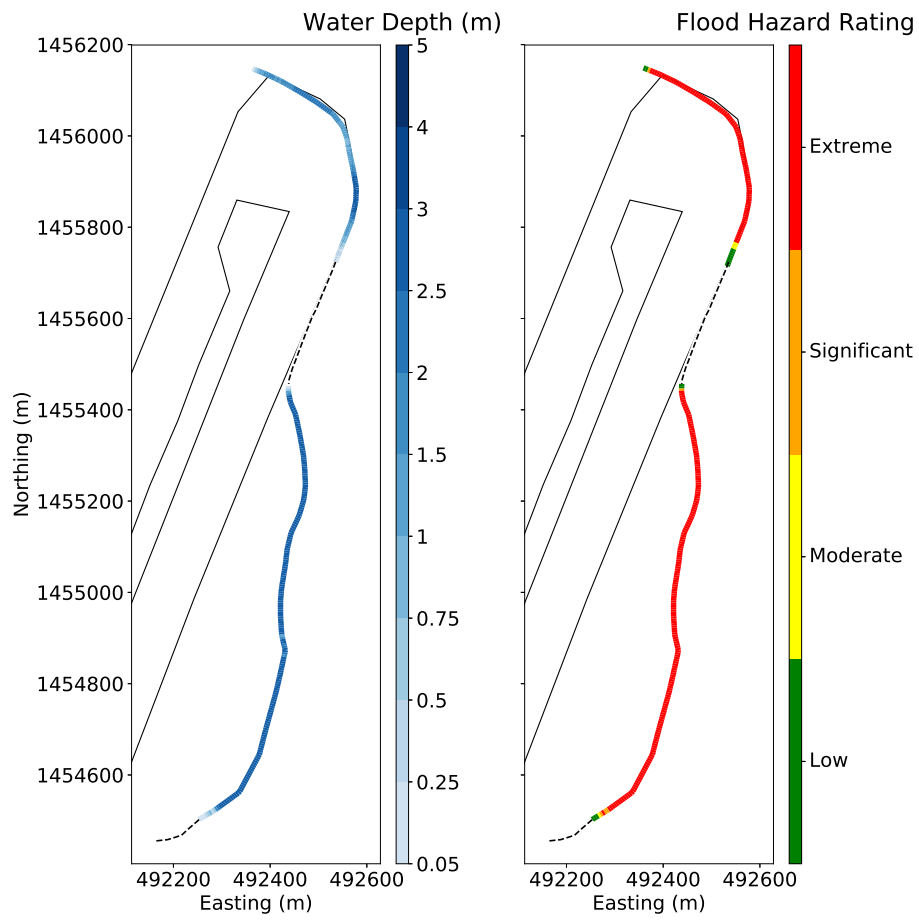


Figure B22: Hydrograph 1, 2500 sea level, tunnel flow constricted by 40%.

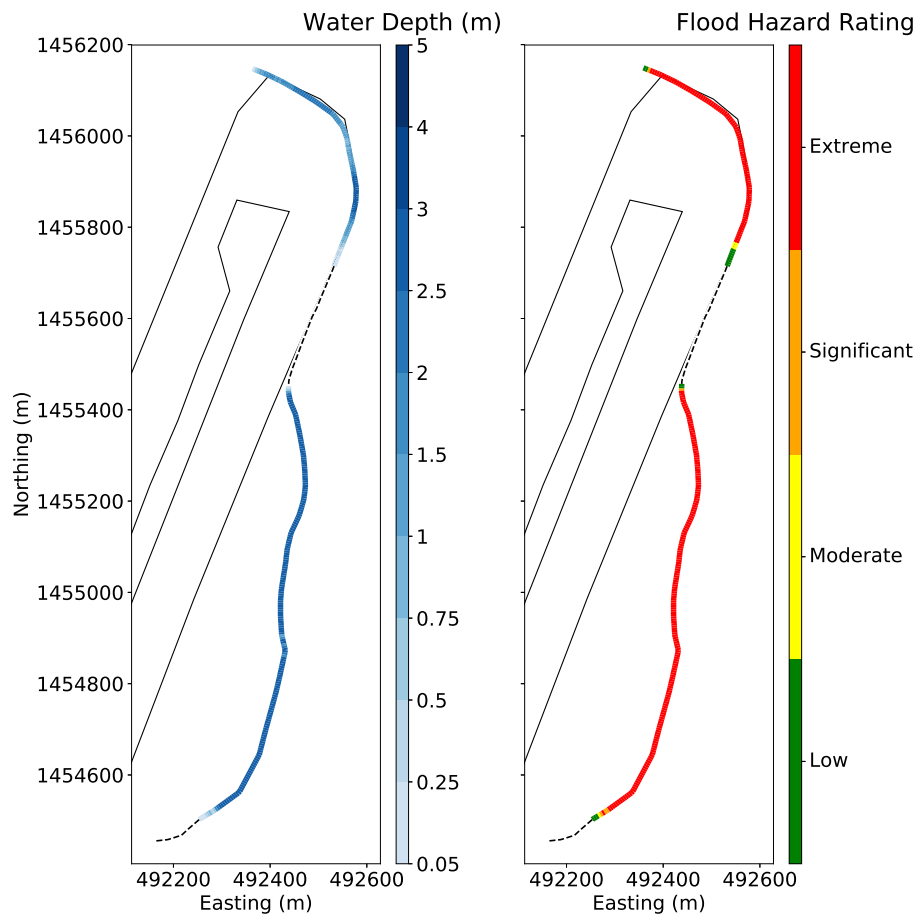


Figure B23: Hydrograph 1, 2500 sea level, tunnel flow constricted by 60%.

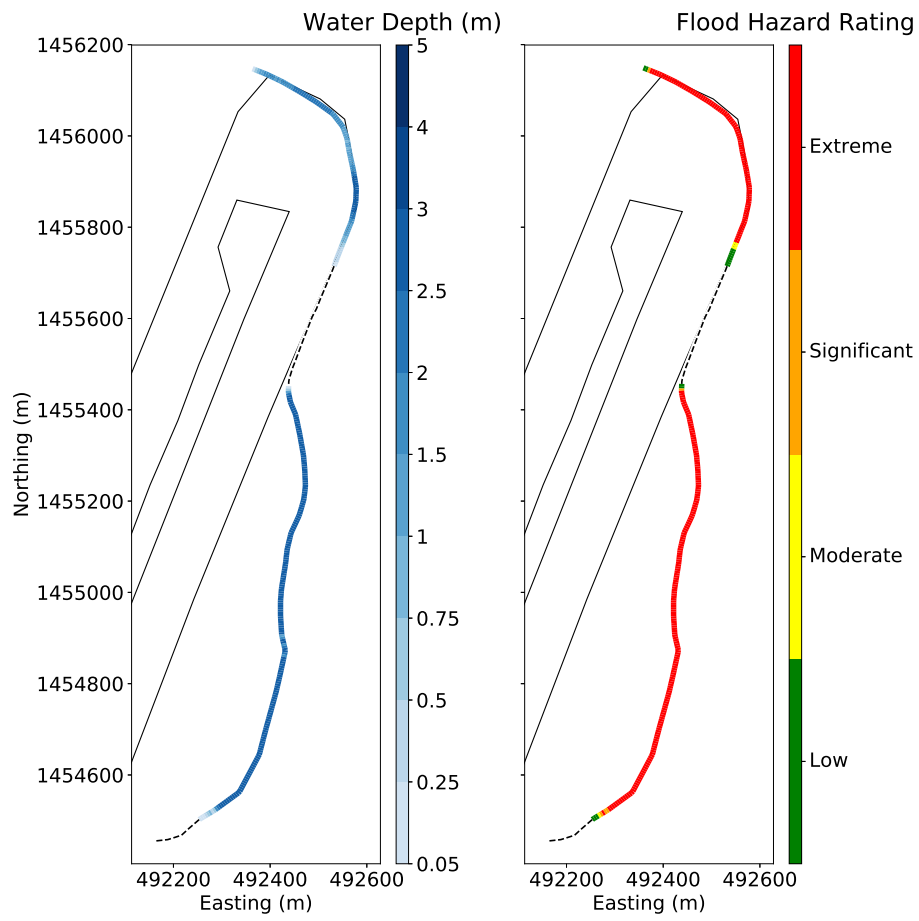


Figure B24: Hydrograph 1, 2500 sea level, tunnel flow constricted by 80%.

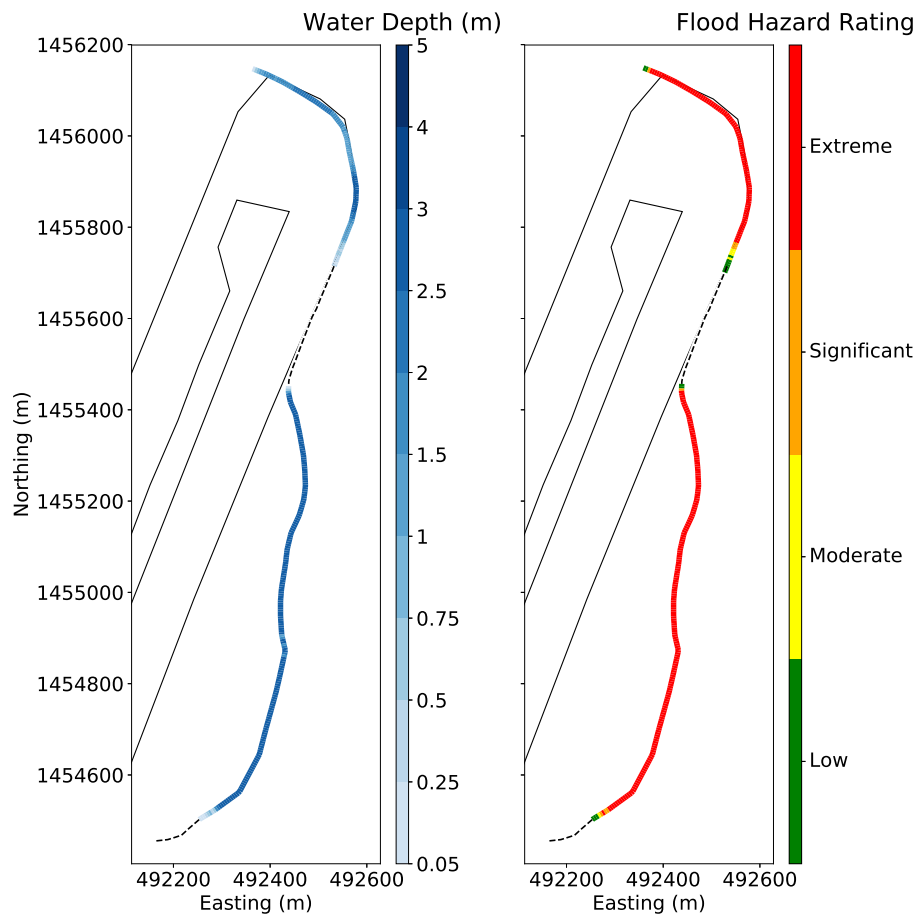


Figure B25: Hydrograph 1, 2500 sea level, tunnel flow constricted by 100%.

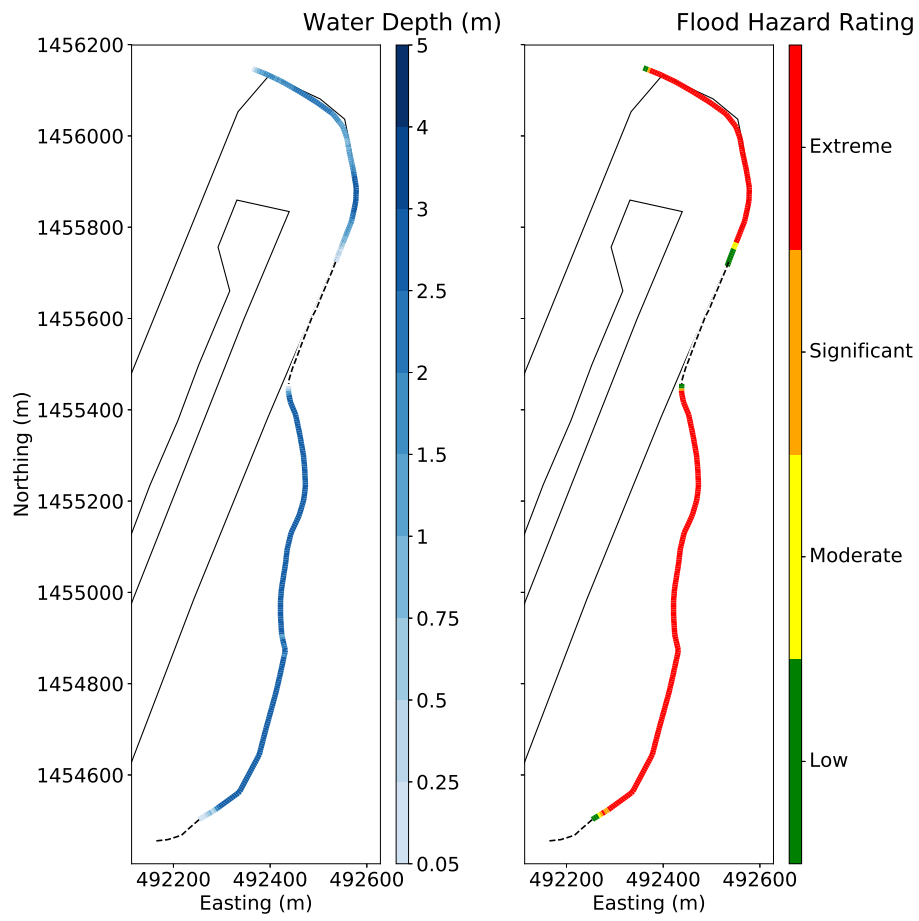


Figure B26: Hydrograph 1, 2500 sea level, tunnel flow constricted by 20%.

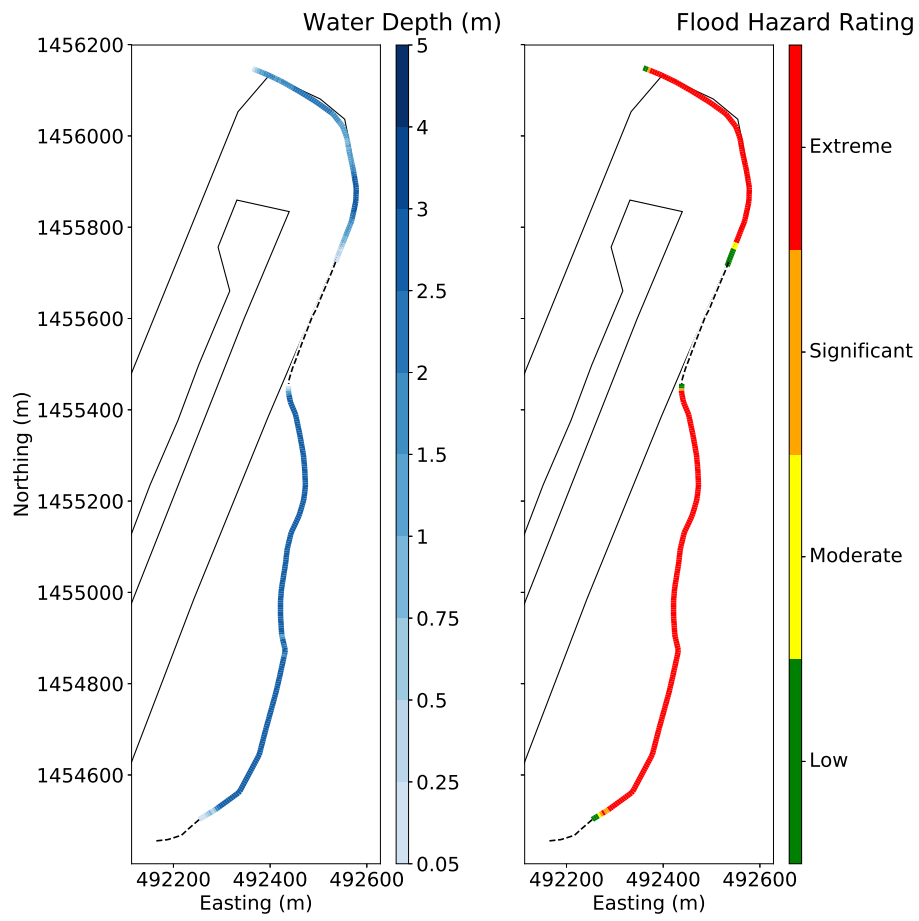


Figure B27: Hydrograph 2, 2500 sea level, tunnel flow constricted by 40%.

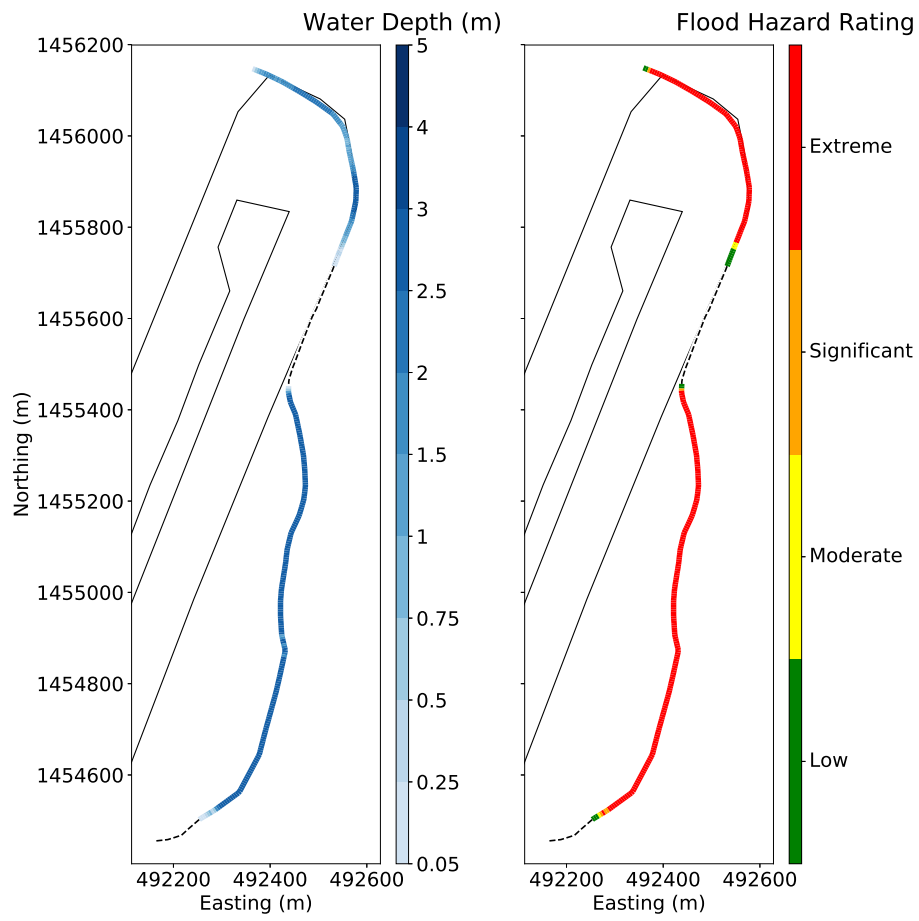


Figure B28: Hydrograph 2, 2500 sea level, tunnel flow constricted by 60%.

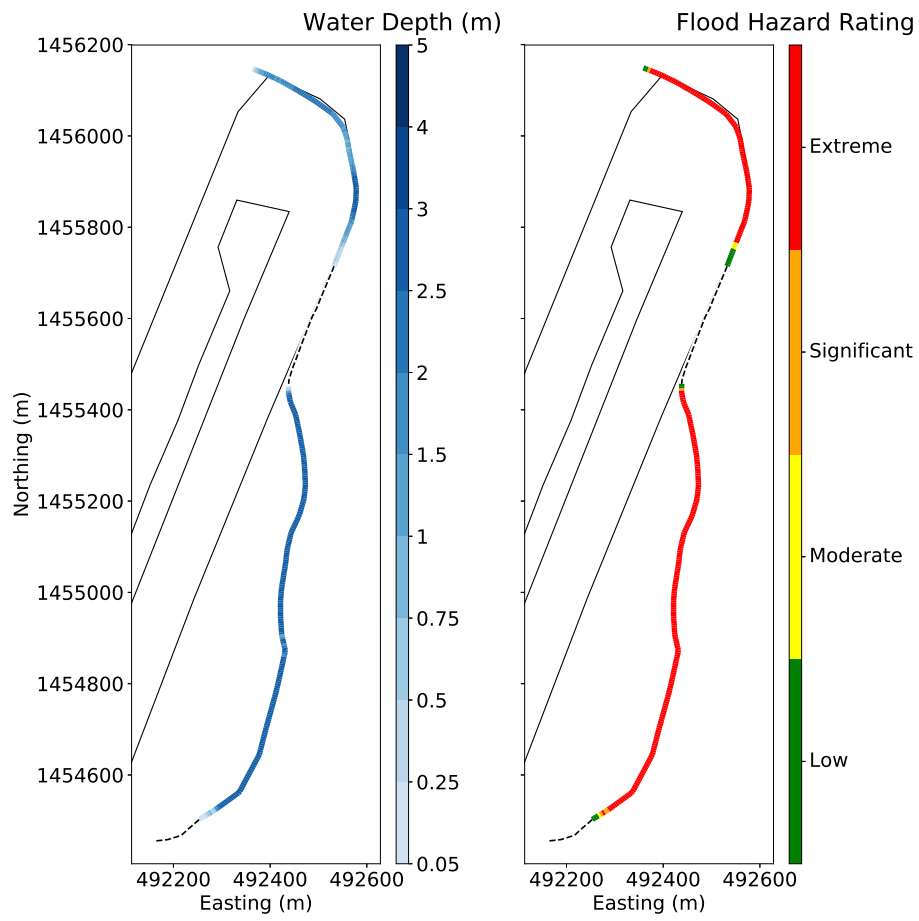


Figure B29: Hydrograph 2, 2500 sea level, tunnel flow constricted by 80%.

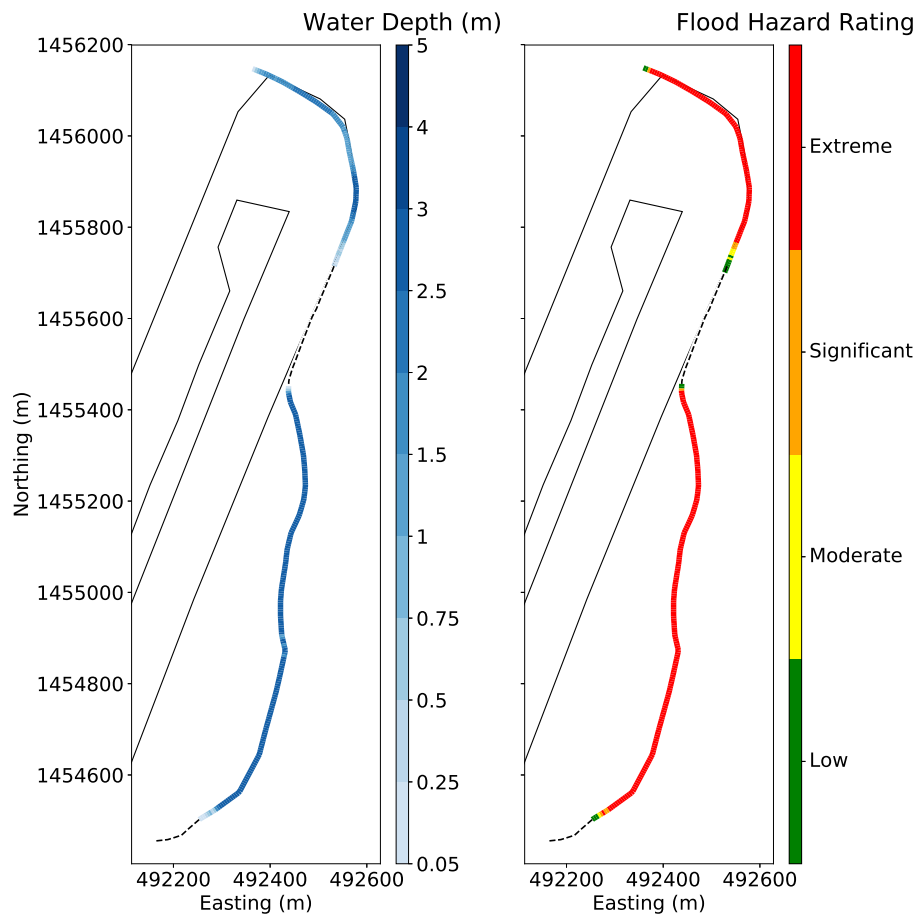


Figure B30: Hydrograph 2, 2500 sea level, tunnel flow constricted by 100%.

C Models and data availability

C.1 XBeach

Basic training in XBeach was delivered to delegates of the Modelling and monitoring for coastal zone management conference and technical workshop held at Kingstown House, Kingstown in January 2019 (National Oceanography Centre, 2019). The workshop tutorial is available here: https://btphillips94.github.io/web_page/cmep-workshop-xbeach.html. Refer to this for information regarding the data requirements for XBeach, which are: beach profile, time series of wave and water level conditions and a setup file. For more details regarding the physics and development of XBeach, refer to this link <https://xbeach.readthedocs.io/en/latest/>. There are also various tutorials available to further demonstrate the capability of XBeach in other types of coastal settings.

C.2 LISFLOOD-FP

LISFLOOD-FP was developed by the Hydrology Group at the University of Bristol. More information and training exercises are available at <http://www.bristol.ac.uk/geography/research/hydrology/models/lisflood/>. The model was referenced at the January 2019 workshop during the XBeach training as a means to use XBeach outputs to model hinterland flooding, but was not covered in detail. Data requirements include:

1. Digital Elevation Model: The spatial resolution depends on your specific research question, for vulnerability studies to specific infrastructure, e.g. AIA's runway, the authors recommend a resolution of no coarser than 5 m. The DEM should cover an area at least to the depth of mean low water.
2. Tide gauge/water level data (if using for a coastal flooding application): This could be either observational data from a tide gauge, or from models, e.g. NEMO and WaveWatchIII with wave setup modelled separately and added to the existing storm tide. These data must be referenced to the same vertical datum as the DEM.
3. River flow data (if using for a fluvial application): This should be supplied as a discharge in cubic metres per second.
4. Rainfall data (if using for a fluvial application and there is no river flow data available): A time series of rainfall in mm per hour.

C.3 Availability of model data

The data used in the modelling studies is stored by the British Oceanographic Data Centre, and is available on request by emailing enquiries@bodc.ac.uk

References

- Bates, P. D., Dawson, R. J., Hall, J. W., Horritt, M. S., Nicholls, R. J., and Wicks, J. Simplified two-dimensional numerical modelling of coastal flooding and example applications. *Coastal Engineering*, 52(9):793–810, 2005. doi: 10.1016/j.coastaleng.2005.06.001.
- Bates, P. D., Horritt, M. S., and Fewtrell, T. J. A simple inertial formulation of the shallow water equations for efficient two-dimensional flood inundation modelling. *Journal of Hydrology*, 387(1-2):33–45, 2010. doi: 10.1016/j.jhydrol.2010.03.027.
- Gallien, T. W., Kalligeris, N., Delisle, M.-P. C., Tang, B.-X., Lucey, J. T. D., and Winters, M. A. Coastal flood modeling challenges in defended urban backshores. *Geosciences*, 8(12), 2018. doi: 10.3390/geosciences8120450.
- Jevrejeva, S., Moore, J., and Grinsted, A. Sea level projections to AD2500 with a new generation of climate change scenarios. *Global and Planetary Change*, 80-81:14 – 20, 2012. doi: <https://doi.org/10.1016/j.gloplacha.2011.09.006>.
- Lichtman, I., Becker, A., Brown, J., and Plater, A. Flood mapping of the island of St. Vincent using ArcGIS. Technical report, University of Liverpool, 2018.
- Longuet-Higgins, M. and Stewart, R. Radiation stresses in water waves; a physical discussion, with applications. *Deep Sea Research and Oceanographic Abstracts*, 11(4):529 – 562, 1964. doi: [https://doi.org/10.1016/0011-7471\(64\)90001-4](https://doi.org/10.1016/0011-7471(64)90001-4).
- National Oceanography Centre. Monitoring and modelling the coastal zone: A 3 day interactive training course and stakeholder workshop. Technical report, 2018.
- National Oceanography Centre. Monitoring and modelling for coastal zone management conference and technical workshop report. Technical report, 2019.
- Prime, T., Brown, J. M., and Plater, A. J. Flood inundation uncertainty: The case of a 0.5% annual probability flood event. *Environmental Science & Policy*, 59:1 – 9, 2016. doi: 10.1016/j.envsci.2016.01.018.
- Roelvink, D., Reniers, A., van Dongeren, A., van Thiel de Vries, J., McCall, R., and Lescinski, J. Modelling storm impacts on beaches, dunes and barrier islands. *Coastal Engineering*, 56(11):1133 – 1152, 2009. doi: <https://doi.org/10.1016/j.coastaleng.2009.08.006>.
- Sampson, C. C., Bates, P. D., Neal, J. C., and Horritt, M. S. An automated routing methodology to enable direct rainfall in high resolution shallow water models. *Hydrological Processes*, 27(3):467–476, 2013. doi: 10.1002/hyp.9515.
- Surendran, S., Gibbs, G., Wade, S., and Udale-Clarke, H. Supplementary note on flood hazard ratings and thresholds- for development planning and control purpose. Technical report, 2008.